ARTICLE

https://doi.org/10.1038/s41586-019-1085-7

# Stem cell competition orchestrates skin homeostasis and ageing

Nan Liu[1,5], Hiroyuki Matsumura[1,5]*, Tomoki Kato[1], Shizuko Ichinose[2], Aki Takada[1], Takeshi Namiki[3], Kyosuke Asakawa[1], Hironobu Morinaga[1], Yasuaki Mohri[1], Adèle De Arcangelis[4], Elisabeth Geroges-Labouesse[4], Daisuke Nanba[1] & Emi K. Nishimura[1]*

**Stem cells underlie tissue homeostasis, but their dynamics during ageing—and the relevance of these dynamics to organ ageing—remain unknown. Here we report that the expression of the hemidesmosome component collagen XVII (COL17A1) by epidermal stem cells fluctuates physiologically through genomic/oxidative stress-induced proteolysis, and that the resulting differential expression of COL17A1 in individual stem cells generates a driving force for cell competition. In vivo clonal analysis in mice and in vitro 3D modelling show that clones that express high levels of COL17A1, which divide symmetrically, outcompete and eliminate adjacent stressed clones that express low levels of COL17A1, which divide asymmetrically. Stem cells with higher potential or quality are thus selected for homeostasis, but their eventual loss of COL17A1 limits their competition, thereby causing ageing. The resultant hemidesmosome fragility and stem cell delamination deplete adjacent melanocytes and fibroblasts to promote skin ageing. Conversely, the forced maintenance of COL17A1 rescues skin organ ageing, thereby indicating potential angles for anti-ageing therapeutic intervention.**

According to the evolutionary theory of ageing, a failure of defence and repair mechanisms leads to the accumulation of damage and thus results in ageing[1,2]. To maintain homeostasis, cells efficiently repair DNA damage and correct spontaneous replication errors[3], and even eliminate mutated cells in tissues. Adult stem cells are vital for replacing cells in tissues, but their capacity declines with age and stem cell exhaustion or the accumulation of senescent cells have previously been implicated in ageing[4,5]. In mammalian hair follicles, dynamic elimination of aged stem cells[6–8] underlies hair ageing phenotypes. However, the exact cellular identity and dynamics of the stressed or damaged cells in large vital organs such as the skin, and their contribution to organ ageing, are largely unknown. In renewing tissues, stem cells undergo 'neutral stem cell competition' by which some somatic stem cells expand clonally while others are lost[9–11]. However, it is unclear whether this process represents neutral drift or the selective elimination of unfit cells through cell competition[12–16].

During epidermal development, epidermal stem cells balance self-renewal and differentiation (stratification) by undergoing two types of cell division: symmetric cell division (SCD), which generates two identical basal daughter cells, and asymmetric cell division, which generates a basal cell and a suprabasal differentiating cell[17,18]. It is unclear how the two are balanced and whether cell competition is involved.

Aged human skin is characterized by atrophy (thinning), fragility, dyspigmentation and delayed wound healing[19–21]. Ageing skin loses its thickness, rete ridges (the reservoir for epidermal keratinocytes[22]) melanocytes and functional dermal fibroblasts[23]. Cutaneous fragility has been partly attributed to changes in hemidesmosomes, structures that directly connect basal keratinocytes to the basement membrane. Indeed, hemidesmosome components such as collagen XVII (COL17A1, also known as BP180 or BPAG2) become downregulated in aged human skin[24,25]. Furthermore, *COL17A1* gene deficiency in humans causes junctional epidermolysis bullosa, which is characterized by skin atrophy and fragility, dyspigmentation and alopecia[26,27]. Consistent with that phenotype, a previous study showed that a *Col17a1* gene deficiency in mice causes skin atrophy with a loss of epidermal stem cell populations[8].

Here we have investigated the involvement and roles of COL17A1 and cell competition in skin homeostasis and ageing by performing in vivo cell fate tracing analysis of epidermal stem cells in mice during ageing and in vitro 3D modelling. We show that *Col17a1*-driven stem cell competition and SCD initially orchestrate skin homeostasis, but that the same mechanisms result in skin ageing later in life.

## Mouse model of mammalian skin ageing

To study mammalian skin ageing, we first histologically analysed mouse tail skin, which consists of well-stratified epidermal cell layers similar to human skin (Fig. 1a, Extended Data Fig. 1a). As in aged human epidermis (Extended Data Fig. 1b, c), aged mouse tail skin shows atrophy, with a reduced number of cell layers in the epidermis (Fig. 1b, c, Extended Data Fig. 1d, e) and basal cells with more flattened morphology (Extended Data Fig. 1f). Both the total number of basal cells and the number of $MCM2^+$ basal cells were reduced by ageing (Extended Data Fig. 1f–h), which indicates that epidermal stem cells and their cell division are diminished by ageing. Ultrastructural analysis revealed that the number of electron-dense plaques (hemidesmosomes) was significantly decreased by ageing (Fig. 1d, e). Micro-delamination of basal cells was found in aged skin but only occasionally in young skin, which suggests that some basal cells are delaminated from the basal layer through the ageing-associated reduction of hemidesmosomes (Fig. 1d, f). We therefore analysed the expression of various hemidesmosome components and integrin β1 (ITGB1) in young and aged tail epidermis. As in aged human epidermis (Extended Data Fig. 1i, j), the expression of COL17A1 was significantly decreased by ageing (Fig. 1g, h, Extended Data Fig. 1k, l). Consistently, immuno-transmission electron

[1]Department of Stem Cell Biology, Medical Research Institute, Tokyo Medical and Dental University, Tokyo, Japan. [2]Research Center for Medical and Dental Sciences, Tokyo Medical and Dental University, Tokyo, Japan. [3]Department of Dermatology, Tokyo Medical and Dental University Graduate School and Faculty of Medicine, Tokyo, Japan. [4]CNRS UMR7104, Inserm U1258, Institut de Génétique et de Biologie Moléculaire et Cellulaire, Development and Stem Cells Department, Université de Strasbourg, Strasbourg, France. [5]These authors contributed equally: Nan Liu, Hiroyuki Matsumura. *e-mail: matsscm@tmd.ac.jp; nishscm@tmd.ac.jp

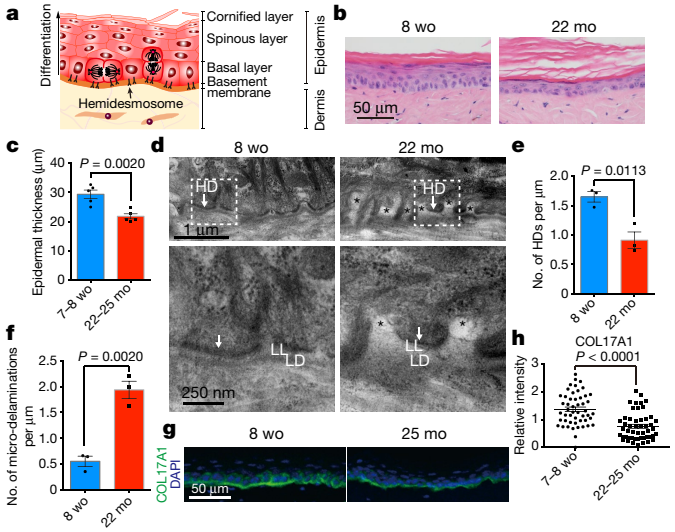


**Fig. 1 | Chronological ageing causes epidermal atrophy with hemidesmosomal instability. a**, Schematic of mouse tail epidermis. Basal cells containing epidermal stem cells are anchored to the basement membrane with hemidesmosomes (black). They divide to duplicate themselves or generate suprabasal daughter cells that commit to differentiation to form the stratified cell layers. **b**, Representative haematoxylin and eosin images of the tail scale areas of 8-week-old (8 wo) and 22-mo wild-type mice. **c**, Quantification of epidermal thickness in tail scale areas from young (7–8 wo, $n = 5$) and aged (22–25 mo, $n = 5$) wild-type mice. **d**, Representative ultrastructural images of epidermal basal cells from young (8 wo) and aged (22 mo) wild-type mice assessed by TEM. Bottom, magnified views of dashed boxed areas. Arrows, hemidesmosomes (HD); asterisks, micro-delaminations; LL, lamina lucida; LD, lamina densa. **e**, **f**, Quantification of the numbers of hemidesmosomes (**e**) and micro-delaminations (**f**) at the basement membrane in tail scale basal cells from young (8 wo, $n = 3$) and aged (22 mo, $n = 3$) mice. **g**, **h**, Representative immunofluorescence images and fluorescence intensities of COL17A1 in tail scale areas from young (7–8 wo, $n = 50$ scales) and aged (22–25 mo, $n = 50$ scales) mice. Means ± s.e.m.; two-tailed *t*-test (**c**, **e**, **f**) or two-tailed Mann–Whitney *U*-test (**h**).

microscopy (TEM) analysis showed a significant decrease in COL17A1 immunogold signals at the dermal–epidermal junction of aged basal epidermis (Extended Data Fig. 1m, n). Whole-mount immunostaining also revealed the heterogeneous distribution of COL17A1 in aged skin (Extended Data Fig. 1o). Notably, COL17A1-negative cell areas that still expressed other components of hemidesmosomes were found (in addition to double-negative cell areas) in the aged tail epidermis, which suggests that the level of COL17A1 protein is the most unstable and that the resulting COL17A1 insufficiency ultimately destabilizes other hemidesmosome components during ageing. We then analysed the stability of those components in human keratinocytes in the presence of the protein synthesis inhibitor cycloheximide (Extended Data Fig. 2a). COL17A1 was the most unstable component of hemidesmosomes (Extended Data Fig. 2b, c) and marimastat—a matrix metalloproteinase inhibitor—stabilized COL17A1 even in the presence of cycloheximide (Extended Data Fig. 2d, e), which indicates that the proteolysis of COL17A1 regulates its stability.

## Genomic stress induces COL17A1 proteolysis

The epidermis suffers various kinds of stress, including replicative and oxidative stress and basement membrane damage by ageing[28,29]. As instability of COL17A1 is induced by ageing or premature ageing[6], we investigated whether such stress triggers the instability of hemidesmosomes in epidermal stem cells. We analysed the expression level of hemidesmosome components in keratinocytes treated with genotoxins (ultraviolet (UV) B, ionizing irradiation and $H_2O_2$). Each of these triggered phosphorylation of γ-H2AX and subsequent downregulation of COL17A1, followed by destabilization of other hemidesmosome components (Extended Data Fig. 2f–l). The UV-induced downregulation of COL17A1 was blocked by marimastat, indicating that genomic stress induces proteolysis of COL17A1 by matrix metalloproteinase and/or ADAMs (a disintegrin and metalloproteinase) (Extended Data Fig. 2m). Similarly, repetitive UV radiation heterogeneously downregulated the expression of COL17A1 in basal keratinocytes (Extended Data Fig. 3a, b) and resulted in hemidesmosome instability in vivo (Extended Data Fig. 3c–f). These data indicate that excessive or repetitive genotoxic stress commonly induces degradation of COL17A1 by triggering the DNA damage response to cause hemidesmosome instability.

As differential COL17A1 expression was found even in young naive epidermis (Fig. 1g, h), we analysed the formation of phospho-replication protein A (p-RPA2/32) foci and the expression of 8-hydroxy-2′-deoxyguanosine (8-OHdG) to detect cells undergoing replicative stress and oxidative DNA damage, respectively[30,31]. Foci of p-RPA2/32 were detected in some basal cells even in young skin (Extended Data Fig. 3g–i) and 8-OHdG$^+$ cells were increased in the basal layer by ageing (Extended Data Fig. 3j, k), as recently reported[28]. Furthermore, the application of hydroxyurea (an inducer of replicative stress) to the skin induced the formation of p-RPA2/32 foci and differential COL17A1 expression in basal and suprabasal cells, followed by a considerable reduction in COL17A1 expression with repetitive hydroxyurea treatment (Extended Data Fig. 3i, l, m). Consistently, COL17A1 was significantly reduced in basal cells with sustained DNA damage response in the aged skin (Extended Data Fig. 3n, o). Finally, we tested whether downregulation of COL17A1 destabilized hemidesmosomes in human keratinocytes. Knockdown of *COL17A1* affected expression of the integrin subunit ITGA6 (Extended Data Fig. 2n, o). Therefore, we conclude that genomic stress induces hemidesmosome instability through proteolysis of COL17A1.

## Clonal expansion of COL17A1$^+$ epidermal stem cells

To visualize the dynamics of stem cell clones with different levels of COL17A1 expression, we generated *K14-creERT2;Rosa26R (R26R)$^{Brainbow2.1}$* mice, which allow the stochastic multi-colour labelling and tracing of epidermal basal cells during ageing (Fig. 2a). After drug induction, cells expressing green, red, yellow or cyan fluorescent proteins (GFP, RFP, YFP or CFP) were found stochastically in whole-mount tail skin from young mice (4.5 months old (mo)) (Fig. 2b), but skin from older mice showed a significant increase in single-coloured clone areas and a decrease in the total number of clones (Fig. 2c, d). This indicates that some stem cells clonally expand at the expense of many others during physiological ageing. To test whether stem cell clone fate is determined stochastically or selectively, we plotted stem cell clone size and the expression of COL17A1. The expression of COL17A1 in basal cells with a single colour, which represents a stem cell clone, in aged skin is generally diminished, whereas in young skin there is conspicuous heterogeneity and a higher level of COL17A1 expression (Fig. 2e). Furthermore, the size of basal cell clones correlated positively with the expression of COL17A1 in aged skin (Fig. 2f), which indicates that COL17A1$^{high}$ stem cells show a higher clonogenic potential to dominate the epidermis. We found no significant induction of apoptosis or accumulation of p16$^+$ cells in the aged epidermis (Extended Data Fig. 4a–d), as previously reported[28]. Collectively, these data indicate that COL17A1$^{high}$ epidermal stem cells are constantly outcompeting COL17A1$^{low}$ cells to eliminate stressed or unfit cells from the skin and thereby to resist epidermal ageing.

## Differential COL17A1 expression triggers competition

To study how COL17A1 mediates cell competition in vivo, we generated drug-inducible *Col17a1* gene knockout (*Col17a1* cKO) mice combined with the multi-colour labelling system specifically in basal keratinocytes (Fig. 2g). Infrequent induction of COL17A1 deficiency allowed us to identify single-colour-labelled *Col17a1*-deficient keratinocyte clones in the tail scale epidermis at day (D) 2 after induction (Fig. 2h). In control mice, these clones increased in size at D14 and

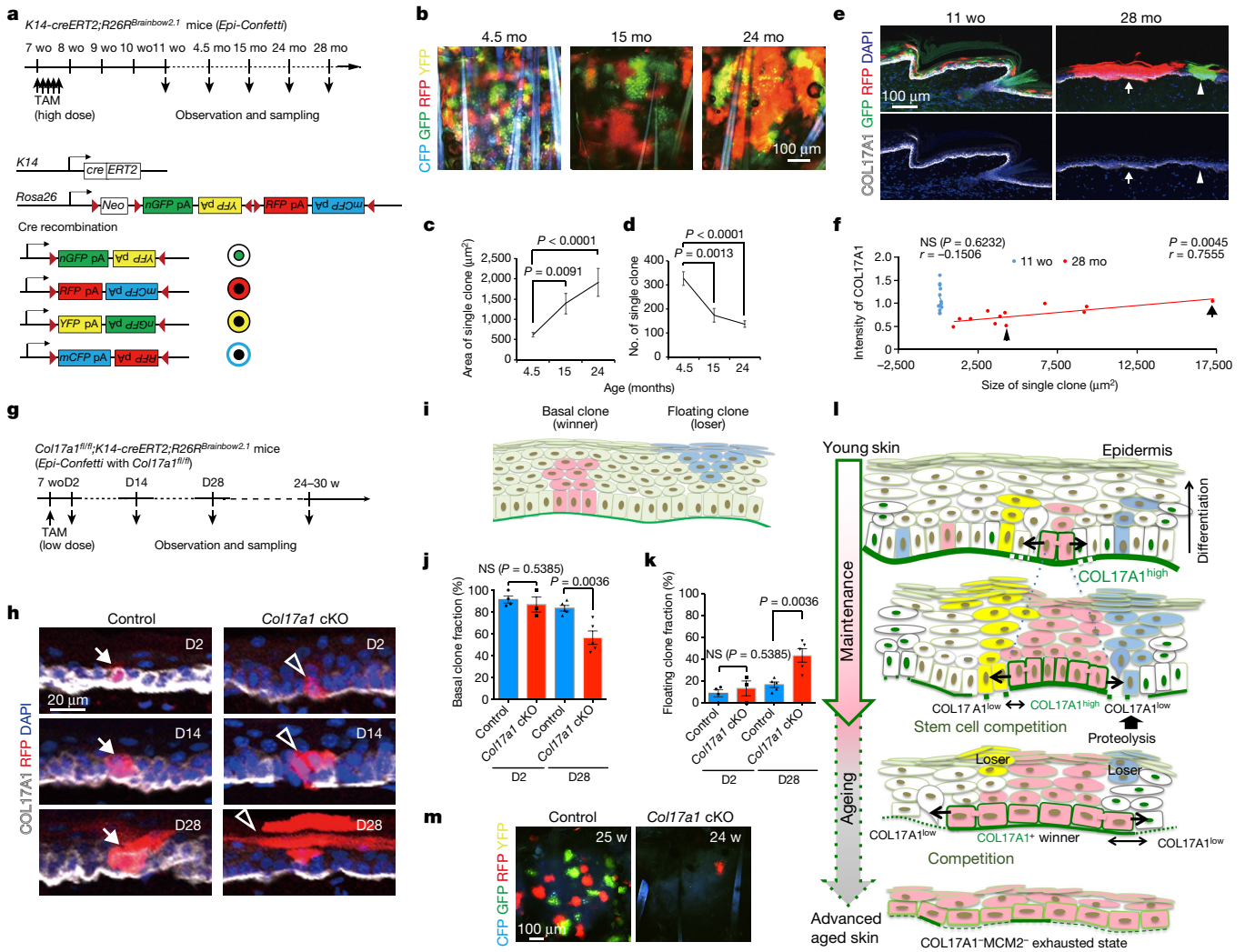


**Fig. 2 | Age-associated differential expression of COL17A1 provokes epidermal stem cell competition. a**, Schematic experimental design for multi-colour fate tracing of epidermal keratinocyte stem and progenitor cells. Seven-week-old *K14-creERT2;R26R*$^{Brainbow2.1}$ homozygous mice (*Epi-Confetti*) were treated with tamoxifen (TAM) for five days (high dose) to label GFP–NLS, RFP, YFP or membrane-bound (m)CFP in epidermal basal cells. At 11 wo and 4.5, 15, 24 and 28 mo, tail skin specimens were collected. **b**, Representative whole-mount images of tail epidermis from young (4.5 mo), middle-aged (15 mo) and aged (24 mo) TAM-treated *Epi-Confetti* mice. **c**, **d**, Quantification of areas ($\mu m^2$; **c**) and numbers (4.5 mo, $n = 5$ images; 15 mo, $n = 4$; 24 mo, $n = 7$; **d**) of single-colour (red) clones in whole-mount images of tail epidermis during ageing. **e**, Representative immunofluorescence images of COL17A1 in multicolour-labelled scale basal keratinocytes from young (11 wo) and aged (28 mo) TAM-treated *Epi-Confetti* mice that were treated with TAM at 10 wo for 5 days. **f**, Quantification of the distribution between COL17A1 intensity and keratinocyte clone size in multiple areas (11 wo, $n = 13$ clones; 28 mo, $n = 12$) of **e**. Arrow, COL17A1$^{mid}$ large clone; arrowhead, COL17A1$^{low}$ small clone (**e**, **f**). *r* is Pearson's correlation coefficient. **g**, Schematic experimental design for stem and progenitor cell fate analysis after COL17A1 deletion. We treated 7-wo *Epi-Confetti* mice with *Col17a1*$^{flox/flox}$ alleles (*Col17a1* cKO) and those without *flox/flox* alleles (control) with TAM for 1 day (low dose) to label basal keratinocytes at clonal density. Skin samples were collected after 2 days (D2), 14 days, 28 days and 24–30 weeks (w). **h**, Representative immunofluorescence images of COL17A1 in RFP-expressing basal cells from control (arrow) and *Col17a1* cKO mice. At D2, COL17A1$^{-}$RFP$^{+}$ basal clones (open arrowhead) appeared in *Col17a1* cKO mice. At D14, those basal clones were delaminated from the basal layer and were surrounded by a COL17A1$^{+}$RFP$^{-}$ clone. At D28, the COL17A1$^{+}$RFP$^{-}$ clone replaced the COL17A1$^{-}$RFP$^{+}$ basal clones and occupied the basal layer. **i**, Schematic of basal cell clones comprising a basal clone (winner) and a floating clone (loser). **j**, **k**, Quantification of basal clones (**j**) and floating clones (**k**) in control (D2, $n = 4$; D28, $n = 5$) and *Col17a1* cKO (D2, $n = 3$; D28, $n = 5$) mice following TAM administration. **m**, Whole-mount images of control and *Col17a1* cKO mice at 24–25 weeks after low-dose TAM (most representative image from two independent experiments). **l**, Schematic of the epidermal ageing program through COL17A1-mediated cell competition. COL17A1$^{high}$ clones (winners) dominate in the basal interfollicular epidermis (IFE), whereas COL17A1$^{low}$ clones (losers) are delaminated from the basal IFE during ageing. Means ± s.e.m.; two-tailed *t*-test (**j**, **k**), one-way ANOVA with Dunnett's post hoc test (**d**) or Kruskal–Wallis test with Dunn's post hoc test (**c**).

formed single-colour clones (basal clones) at D28[32] (Fig. 2h, i). By contrast, many *Col17a1*$^{-}$ basal clones were surrounded by non-labelled COL17A1$^{+}$ clones at D14 and then delaminated as loser cell clones (floating clones) by D28 (Fig. 2h–k). These *Col17a1*$^{-}$ loser clones were delaminated, forming multiple cell layers after their sequential cell divisions without showing any significant induction of cell death (Extended Data Fig. 5a–k). Consistently, both *Col17a1*$^{-}$ and *Col17a1*$^{+/-}$ clones were significantly eliminated by surrounding COL17A1$^{+}$ cells and disappeared from the skin (Fig. 2m, Extended Data Fig. 5l–n). These data indicate that differential COL17A1 expression by individual stem cells drives cell–cell competition in a cell-division-coupled manner (Fig. 2l).

To model stem cell competition in vitro, we established an assay system with 3D-cultured keratinocyte sheets using the HaCaT human

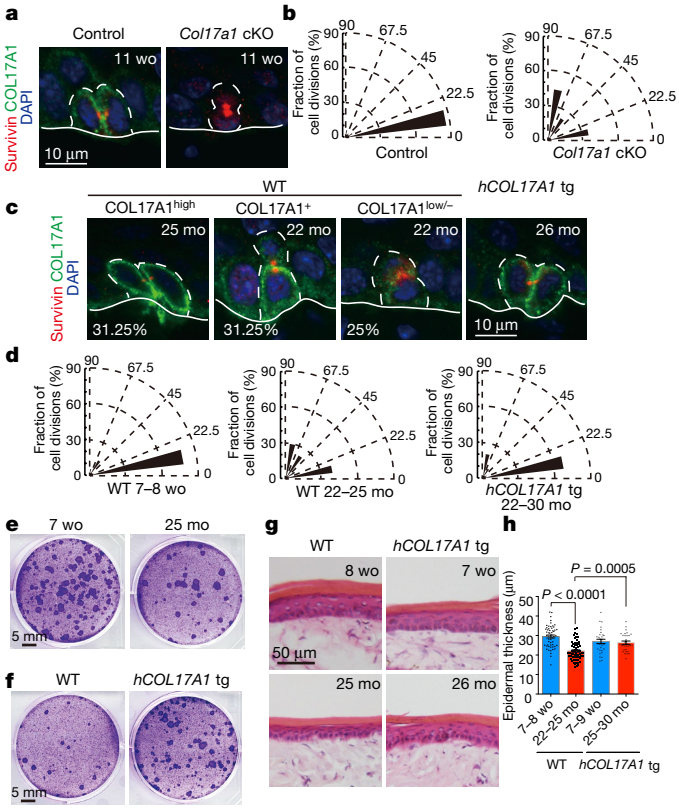


**Fig. 3 | Epidermal homeostasis is maintained by COL17A1-mediated symmetric cell divisions. a**, **c**, Representative immunofluorescence images of survivin and COL17A1 in epidermal basal cells from control (11 wo, wild-type (WT)) and *Col17a1* cKO (11 wo) mice (**a**) or from aged (22–25 mo) wild-type mice and aged (26 mo) *hCOL17A1* tg mice (**c**). Survivin (red) concentrates at the cleavage furrow in telophase. Solid lines, basement membrane; dashed lines, cell boundary. **b**, **d**, Radial histogram quantification of division angles in epidermal basal cells from control (11 wo, $n = 4$) and *Col17a1* cKO (11 wo, $n = 3$) mice (**b**) or from young (7–8 wo, $n = 5$) or aged (22–25 mo, $n = 4$) wild-type mice and aged *hCOL17A1* tg (22–30 mo, $n = 5$) mice (**d**). Mean frequency of expression of COL17A1$^{high}$ (left), COL17A1$^{+}$ (middle left) or COL17A1$^{low/-}$ (middle right) from aged wild-type mice ($n = 3$) is shown at the bottom (**c**). **e**, **f**, Colony-forming analysis of tail epidermal keratinocytes from young (7 wo, $n = 3$) and aged (25 mo, $n = 3$) mice (**e**) or from wild-type (8 wo, $n = 3$) and *hCOL17A1* tg (8 wo, $n = 3$) mice (**f**). **g**, Representative haematoxylin and eosin images of tail scale area from 7–8-wo and 25–26-mo wild-type mice and from *hCOL17A1* tg mice. **h**, Quantification of epidermal thickness in the tail scale area from young and aged wild-type mice (7–8 wo, $n = 55$ epidermises; 22–25 mo, $n = 61$) and from *hCOL17A1* tg mice (7–9 wo, $n = 30$; 25–30 mo, $n = 30$). Means ± s.e.m.; one-way ANOVA with Dunnett's post hoc test (**h**).

keratinocyte cell line (Extended Data Fig. 6a). We introduced an emerald green fluorescent protein (EmGFP) and a short hairpin RNA (shRNA) construct (either targeting *COL17A1* or scrambled) into HaCaT cells, and then 3D-cultured them (Extended Data Fig. 6a). There was no clear difference in structure, stratification or the number of proliferating or apoptotic cells in the 3D-cultured epidermis between shScramble- and sh*COL17A1*-expressing HaCaT cells (Extended Data Fig. 6b–f). On the other hand, co-cultures of COL17A1$^{-}$ cells with COL17A1$^{+}$ cells at a 1:10 ratio—but not at a 1:3 ratio—significantly eliminated the COL17A1$^{-}$ cells (Extended Data Fig. 6g–k). Thus, *Col17a1*-deficient basal cells are eliminated from the skin as loser cells when surrounded by a sufficient number of COL17A1$^{+}$ cells (Fig. 2l).

## COL17A1–mediated SCDs drive stem cell competition

To understand how COL17A1$^{+}$ stem cells eliminate COL17A1$^{-}$ cells, we analysed the division axes of basal cells in vivo. Whereas control basal cells mostly showed parallel cell divisions against the basement membrane in adult skin, *Col17a1*$^{-}$ basal cells underwent perpendicular asymmetric cell divisions to generate a basal cell and an apically located differentiating suprabasal cell (Fig. 3a, b). This indicates that COL17A1 mediates SCDs and suggests that the COL17A1-mediated SCDs mechanistically push out *Col17a1*$^{-}$ basal cells with reduced numbers of hemidesmosomes to be micro-detached from the basement membrane. Indeed, *Col17a1*$^{-}$ keratinocytes are eventually delaminated from the epidermis (Fig. 2m). Therefore, the COL17A1-dependent SCDs that promote the clonal expansion of COL17A1$^{+}$ winner cells drive cell competition during ageing. Notably, basal cells in the aged epidermis showed an increased ratio of perpendicular cell divisions, often with lower expression of COL17A1 (Fig. 3c, d). However, this eventually causes epidermal thinning with impaired cell divisions and the loss of COL17A1 and MCM2 expression in advanced aged skin (Extended Data Figs. 1f–h, 2l). By contrast, epidermal basal cells in *COL17A1* transgenic (*hCOL17A1* tg) mice—in which basal cells maintain COL17A1 expression[33]—maintained parallel cell divisions (Fig. 3c, d). These data indicate that COL17A1-mediated SCDs generate the mechanical driving force for cell competition through their horizontal spread and resulting occupancy of the basement membrane zone in the adult epidermis to resist epidermal ageing.

To test whether COL17A1-mediated SCDs sustain the clonal expansion of epidermal stem cell clones, we used a colony-formation assay, the gold standard in vitro self-renewal assay[34]. Aged COL17A1$^{low}$ epidermal keratinocytes had a decreased colony-forming ability and also produced smaller colonies than younger keratinocytes (Fig. 3e, Extended Data Fig. 7a, b). By contrast, the forced expression of *hCOL17A1* by basal keratinocytes in mice[33] promoted clonogenic potential, which resulted in a significantly larger colony size and number than in control mice (Fig. 3f, Extended Data Fig. 7c, d). These data indicate that COL17A1 mediates clonal expansion through the outgrowing capabilities of epidermal stem cells. Consistently, expression of the *hCOL17A1* transgene in mice significantly rescued age-associated epidermal thinning (Fig. 3g, h), age-associated micro-delamination and the flattened shape of basal cells (Extended Data Fig. 7e–g). Furthermore, a COL17A1$^{+}$ population of human keratinocytes purified by fluorescent-activated cell sorting (FACS) showed a high clonogenic potential, whereas the COL17A1$^{low/-}$ population generated a reduced number of small colonies (Extended Data Fig. 7h, i). The COL17A1-dependent self-renewal of epidermal stem cells by parallel SCDs explains the higher fitness of COL17A1$^{+}$ stem cell clones in cell competition during tissue homeostasis and ageing.

## Heterotypic lineage ageing by epidermal stem ageing

To study the functional relevance of epidermal stem cell ageing in skin ageing, we first assessed skin dyspigmentation. As shown in Fig. 4a, physiological ageing gradually provokes skin dyspigmentation (heterogeneous hypo- and hyper-pigmentation) and finally induces hypo-pigmentation in the tail skin. Detailed microscopic observation of whole-mount tail scales revealed that the pigmentation pattern became heterogeneous during ageing (Extended Data Fig. 8a, b). Microarray analysis of young and aged total epidermal cells also ranked melanocytic genes as the top major changes during ageing (Extended Data Fig. 8c, d). To visualize the distribution of melanocyte lineage cells in the epidermis, we analysed the tail skin of *Dct-H2B-GFP* tg mice, in which H2B–GFP is expressed in the melanocyte lineage[35] (Extended Data Fig. 8e). Cross-section and whole-mount analyses showed that H2B–GFP$^{+}$ epidermal melanoblasts and melanocytes in the tail scales of young mice had disappeared in aged tail epidermis (Fig. 4b, c, Extended Data Fig. 8f, g). Furthermore, analysis of 13–14-mo *K14-creERT2;R26R*$^{Brainbow2.1}$ mice identified highly pigmented melanocytes attached to floating clones in the suprabasal layer of tail skin (Fig. 4b, d), which indicates that these differentiated melanocytes are co-delaminated from the basal layer together with adherent or surrounding keratinocytes. Consistently, the hemidesmosome instability triggered by *Col17a1* deficiency also induced relatively mild

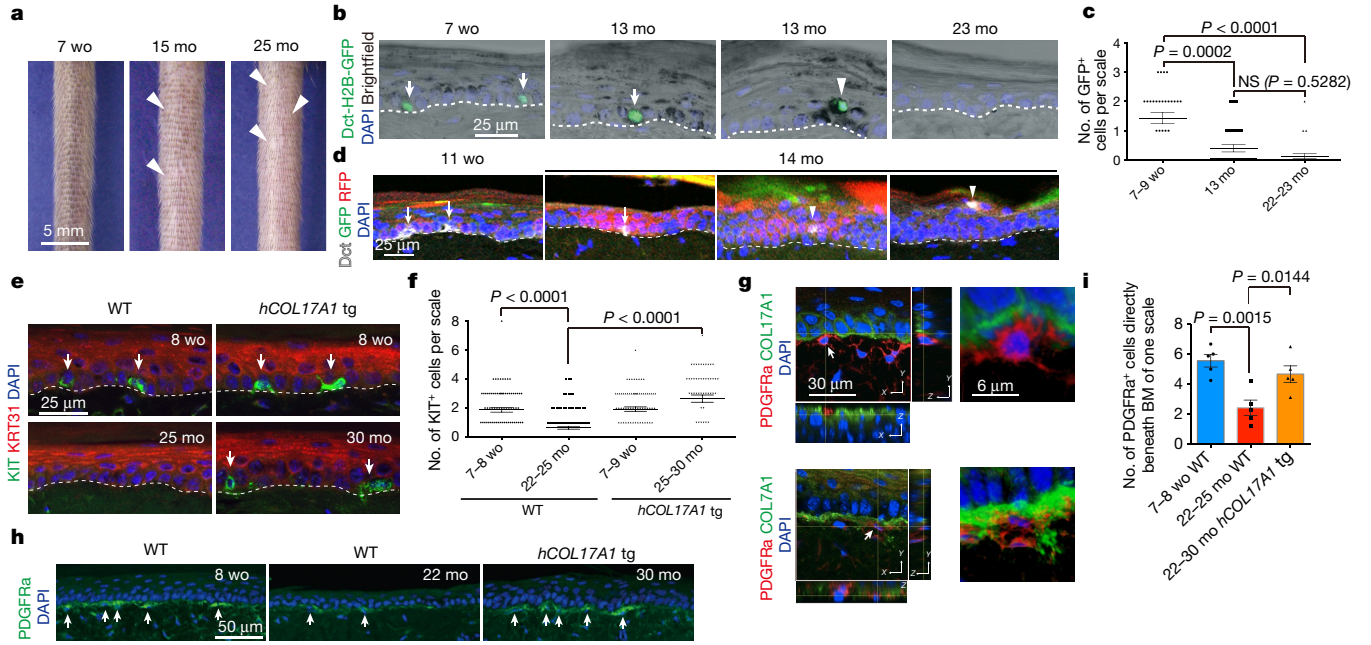


**Fig. 4 | Heterotypic lineage maintenance in the skin by COL17A1$^+$ epidermal stem cells. a**, Representative chronological changes of tail skin pigmentation in 7-wo (young), 15-mo (middle-aged) and 25-mo (aged) wild-type mice. Arrowheads, hypo-pigmentation during ageing. Representative of at least five independent experiments. **b**, Representative combined images of fluorescent and bright-field views of GFP-marked melanocytes (arrows) in 7-wo, 13-mo and 23-mo *Dct-H2B-GFP* tg mice. Arrows, epidermal melanoblasts or melanocytes; arrowhead, a pigmented dendritic melanocyte delaminating from the basal layer. **c**, Number of GFP-marked melanocytes per scale area from young (7–9 wo, $n = 30$ scales), middle-aged (13 mo, $n = 30$) and aged (22–23 mo, $n = 30$) mice. **d**, Representative immunofluorescence images for DCT, a marker of the melanocyte lineage, in multicolour-labelled scale basal keratinocytes from young (11 wo) and middle-aged (14 mo) TAM-treated *Epi-Confetti* mice. In young mice, melanocytes were maintained among scale IFE (arrows), whereas in middle-aged mice melanocytes were occasionally co-delaminated with basal clone (arrowheads). **e**, Representative immunofluorescence images of KRT31 and KIT expression by wild-type and *hCOL17A1* tg mice at 8 wo and 25–30 mo. Arrows, epidermal melanocytes among tail scale basal keratinocytes. **f**, Number of KIT$^+$ epidermal melanocytes per scale area from young and aged wild-type mice (7–8 wo, $n = 86$ scales; 22–25 mo, $n = 134$) and from young and aged *hCOL17A1* tg mice (7–9 wo, $n = 81$; 25–30 mo, $n = 60$) mice. **g**, Representative 3D reconstructed immunofluorescence images of PDGFRa$^+$ dermal fibroblasts and COL17A1$^+$/COL7A1$^+$ epidermal keratinocytes. Arrows, close contacts between fibroblasts and keratinocytes. **h**, Immunofluorescence images of PDGFRa$^+$ dermal fibroblasts from young (8 wo) and aged (22 mo) wild-type mice and from aged (30 mo) *hCOL17A1* tg mice. **i**, Number of PDGFRa$^+$ dermal fibroblasts in young (7–8 wo, $n = 5$) and aged (22–25 mo, $n = 5$) wild-type mice and in aged *hCOL17A1* tg (22–30 mo, $n = 5$) mice. Expression of the *hCOL17A1* transgene significantly rescued the depletion of PDGFRa$^+$ dermal cells (arrows) beneath the basement membrane (BM). Similar results were obtained in at least three separate samples (**d**, **g**). Dashed lines, basement membrane. Mean ± s.e.m.; Kruskal–Wallis test with Dunn's post hoc test (**c**, **f**) or one-way ANOVA with Dunnett's post hoc test (**i**).

dyspigmentation, whereas combined deficiencies in *Col17a1* and *Itga6* synergistically induced a more notable dyspigmentation and melanocyte depletion (Extended Data Fig. 8h–k).

Chronic UVB irradiation causes skin photoageing with dyspigmentation and hemidesmosome damage in mouse and human epidermis[36,37]. Repeated UVB exposure induces skin hyperpigmentation followed by the appearance of hypopigmented spots, similarly to *Col17a1* or *Itga6* cKO mice (Extended Data Fig. 8h, l), with impairment of the formation of mature hemidesmosomes and a decrease in COL17A1 immunogold signals (Extended Data Fig. 8m, n). Moreover, overexpression of *COL17A1* in basal keratinocytes of mice significantly rescued macro- and microscopic dyspigmentation phenotypes and also the age-associated reduction in KIT$^+$ epidermal melanocytes (Fig. 4e, f, Extended Data Fig. 8o). Together, these data show that epidermal melanocytes are maintained by adjacent COL17A1$^+$ epidermal stem cells during chronological ageing and photoageing.

We next analysed the epidermal–dermal junction and found that PDGFRa$^+$ fibroblasts beneath the basement membrane form special junctional structures that support COL17A1$^+$ epidermal basal cells (Fig. 4g), and that the anchoring structures are significantly decreased by ageing. Furthermore, the forced expression of *hCOL17A1* rescued the age-associated disappearance of PDGFRa$^+$ cells and junctional structures (Fig. 4h, i). Thus, COL17A1-mediated epidermal stem cell maintenance resists skin organ ageing through heterotypic cell maintenance.

## Epidermal competition for organ regeneration

Skin wound healing requires massive clonal expansion of epidermal stem cells[38]. To test whether COL17A1-mediated stem cell expansion mediates this process, but declines during ageing, we performed full-thickness wound-healing experiments using the tail skin[39] of wild-type mice. Measurements of wound areas showed that both physiological ageing and *Col17a1*- or *Itga6*- deficiencies in mice significantly delayed wound healing (Extended Data Fig. 9a–f), which demonstrates that the instability of hemidesmosomes leads to defective wound healing in physiological ageing. Notably, the forced expression of *hCOL17A1* by basal keratinocytes in mice[33] promoted wound healing (Extended Data Fig. 9a, g, h). Therefore, the COL17A1-mediated clonal expansion of epidermal stem cells is also essential for the regeneration of full-thickness skin during wound healing.

Because the overexpression of COL17A1 facilitates skin wound healing, we searched for chemical compounds that would induce COL17A1 expression in keratinocytes in vitro. As shown in Extended Data Fig. 9i–l, we identified two chemicals—Y27632 and apocynin—that induced COL17A1 expression in keratinocytes. To test whether these compounds increased the self-renewing capabilities of epidermal stem cells in vitro, we performed colony-formation assays[40,41]; Y-27632 increased colony number, and both drugs increased colony size (Extended Data Fig. 9m–p). Application of these drugs to full-thickness skin wounds significantly promoted wound repair, similarly to the effect of overexpression of

human COL17A1 in mice (Extended Data Fig. 9q–s). Collectively, these data show that COL17A1-inducing drugs promote skin wound healing through re-epithelization of the wound edge with epidermal stem cell expansion, and point towards directions for facilitating skin regeneration and reducing skin ageing.

## Discussion

This study focused on cell-to-cell variability in epidermal stem cells and revealed that differential COL17A1 expression generated by genomic or oxidative stress in adjacent epidermal stem cells drives stem cell competition through COL17A1-dependent SCDs. Parallel cell divisions that spread horizontally on the basement membrane naturally generate the mechanical driving force for cell competition via spatial constraints to eliminate stressed cells with fewer hemidesmosomes in the basal layer, but this competition process eventually declines (Extended Data Fig. 10). COL17A1 is thus not only a good marker for epidermal stem cells but also reflects individual cellular potential and quality for self-renewal. We previously proposed the concept of a 'self-renewal checkpoint' that limits the self-renewal of stem cells under genotoxic stress[6,42]. Our present data indicate that stress-induced COL17A1 proteolysis mediates the checkpoint function for natural selection of qualified stem cells for life-long organ homeostasis.

Ultimately, the advanced aged epidermis consists of immature basal cells in a $COL17A1^{-}MCM2^{-}$ non-competitive state (Fig. 1, Extended Data Fig. 4). Such skin erodes easily because of its fragility, and wound re-epithelization is impaired, mimicking the skin of *COL17A1*-deficient patients and mice[8]. Meanwhile, a notable phenomenon called 'natural gene therapy' (revertant mosaicism) has been found in *COL17A1*-deficient patients[43–45]. It is characterized by natural skin replacement by COL17A1-revertant cells with marked functional and structural recovery and rejuvenation, and is likely to be based on the physiological cell competition mechanism. Furthermore, hemidesmosome-mediated epidermal stem cell maintenance is essential for the maintenance of adjacent melanocytes and fibroblasts to prevent skin ageing. Collectively, our data show that cell competition coupled with SCDs is crucial for mammalian epithelial organ youthfulness, homeostasis with quality control and eventual ageing, providing insights into other epithelial organs. Small molecules that stabilize COL17A1 promote skin wound healing, and may therefore be beneficial for organ integrity, regeneration and the reduction of ageing.

## Online content

Any methods, additional references, Nature Research reporting summaries, source data, statements of data availability and associated accession codes are available at https://doi.org/10.1038/s41586-019-1085-7.

Received: 27 March 2018; Accepted: 7 March 2019;
Published online: 03 April 2019

1. Medawar, P. B. *An Unsolved Problem of Biology* (Published for the College by H. K. Lewis, 1952).
2. Kirkwood, T. Ageing: too fast by mistake. *Nature* **444**, 1015–1017 (2006).
3. Martincorena, I. & Campbell, P. J. Somatic mutation in cancer and normal cells. *Science* **349**, 1483–1489 (2015).
4. van Deursen, J. M. The role of senescent cells in ageing. *Nature* **509**, 439–446 (2014).
5. Goodell, M. A. & Rando, T. A. Stem cells and healthy aging. *Science* **350**, 1199–1204 (2015).
6. Matsumura, H. et al. Hair follicle aging is driven by transepidermal elimination of stem cells via COL17A1 proteolysis. *Science* **351**, aad4395 (2016).
7. Nishimura, E. K., Granter, S. R. & Fisher, D. E. Mechanisms of hair graying: incomplete melanocyte stem cell maintenance in the niche. *Science* **307**, 720–724 (2005).
8. Tanimura, S. et al. Hair follicle stem cells provide a functional niche for melanocyte stem cells. *Cell Stem Cell* **8**, 177–187 (2011).
9. Snippert, H. J. et al. Intestinal crypt homeostasis results from neutral competition between symmetrically dividing Lgr5 stem cells. *Cell* **143**, 134–144 (2010).
10. Stine, R. R. & Matunis, E. L. Stem cell competition: finding balance in the niche. *Trends Cell Biol*. **23**, 357–364 (2013).
11. Clayton, E. et al. A single type of progenitor cell maintains normal epidermis. *Nature* **446**, 185–189 (2007).
12. Morata, G. & Ripoll, P. Minutes: mutants of *Drosophila* autonomously affecting cell division rate. *Dev. Biol*. **42**, 211–221 (1975).
13. Vincent, J. P., Fletcher, A. G. & Baena-Lopez, L. A. Mechanisms and mechanics of cell competition in epithelia. *Nat. Rev. Mol. Cell Biol*. **14**, 581–591 (2013).
14. Merino, M. M., Levayer, R. & Moreno, E. Survival of the fittest: essential roles of cell competition in development, aging, and cancer. *Trends Cell Biol*. **26**, 776–788 (2016).
15. Clavería, C. & Torres, M. Cell competition: mechanisms and physiological roles. *Annu. Rev. Cell Dev. Biol*. **32**, 411–439 (2016).
16. Maruyama, T. & Fujita, Y. Cell competition in mammals—novel homeostatic machinery for embryonic development and cancer prevention. *Curr. Opin. Cell Biol*. **48**, 106–112 (2017).
17. Williams, S. E., Beronja, S., Pasolli, H. A. & Fuchs, E. Asymmetric cell divisions promote Notch-dependent epidermal differentiation. *Nature* **470**, 353–358 (2011).
18. Poulson, N. D. & Lechler, T. Asymmetric cell divisions in the epidermis. *Int. Rev. Cell Mol. Biol*. **295**, 199–232 (2012).
19. Kurban, R. S. & Bhawan, J. Histologic changes in skin associated with aging. *J. Dermatol. Surg. Oncol*. **16**, 908–914 (1990).
20. Farage, M. A., Miller, K. W. & Maibach, H. I. *Textbook of Aging Skin* (Springer, 2010).
21. Gosain, A. & DiPietro, L. A. Aging and wound healing. *World J. Surg*. **28**, 321–326 (2004).
22. Giangreco, A., Goldie, S. J., Failla, V., Saintigny, G. & Watt, F. M. Human skin aging is associated with reduced expression of the stem cell markers β1 integrin and MCSP. *J. Invest. Dermatol*. **130**, 604–608 (2010).
23. Mine, S., Fortunel, N. O., Pageon, H. & Asselineau, D. Aging alters functionally human dermal papillary fibroblasts but not reticular fibroblasts: a new view of skin morphogenesis and aging. *PLoS ONE* **3**, e4066 (2008).
24. Langton, A. K., Halai, P., Griffiths, C. E., Sherratt, M. J. & Watson, R. E. The impact of intrinsic ageing on the protein composition of the dermal-epidermal junction. *Mech. Ageing Dev*. **156**, 14–16 (2016).
25. Watanabe, M. et al. Type XVII collagen coordinates proliferation in the interfollicular epidermis. *eLife* **6**, e26635 (2017).
26. McGrath, J. A. et al. Mutations in the 180-kD bullous pemphigoid antigen (BPAG2), a hemidesmosomal transmembrane collagen (COL17A1), in generalized atrophic benign epidermolysis bullosa. *Nat. Genet*. **11**, 83–86 (1995).
27. Jonkman, M. F. et al. 180-kD bullous pemphigoid antigen (BP180) is deficient in generalized atrophic benign epidermolysis bullosa. *J. Clin. Invest*. **95**, 1345–1352 (1995).
28. Solanas, G. et al. Aged stem cells reprogram their daily rhythmic functions to adapt to stress. *Cell* **170**, 678–692.e20 (2017).
29. Amano, S. Characterization and mechanisms of photoageing-related changes in skin. Damages of basement membrane and dermal structures. *Exp. Dermatol*. **25** (Suppl. 3), 14–19 (2016).
30. Zeman, M. K. & Cimprich, K. A. Causes and consequences of replication stress. *Nat. Cell Biol*. **16**, 2–9 (2014).
31. Bartkova, J. et al. Replication stress and oxidative damage contribute to aberrant constitutive activation of DNA damage signalling in human gliomas. *Oncogene* **29**, 5095–5102 (2010).
32. Mascré, G. et al. Distinct contribution of stem and progenitor cells to epidermal maintenance. *Nature* **489**, 257–262 (2012).
33. Olasz, E. B. et al. Human bullous pemphigoid antigen 2 transgenic skin elicits specific IgG in wild-type mice. *J. Invest. Dermatol*. **127**, 2807–2817 (2007).
34. Langton, A. K., Herrick, S. E. & Headon, D. J. An extended epidermal response heals cutaneous wounds in the absence of a hair follicle stem cell contribution. *J. Invest. Dermatol*. **128**, 1311–1318 (2008).
35. Ueno, M., Aoto, T., Mohri, Y., Yokozeki, H. & Nishimura, E. K. Coupling of the radiosensitivity of melanocyte stem cells to their dormancy during the hair cycle. *Pigment Cell Melanoma Res*. **27**, 540–551 (2014).
36. Amano, S. Possible involvement of basement membrane damage in skin photoaging. *J. Investig. Dermatol. Symp. Proc*. **14**, 2–7 (2009).
37. Inomata, S. et al. Possible involvement of gelatinases in basement membrane damage and wrinkle formation in chronically ultraviolet B-exposed hairless mouse. *J. Invest. Dermatol*. **120**, 128–134 (2003).
38. Aragona, M. et al. Defining stem cell dynamics and migration during wound healing in mouse skin epidermis. *Nat. Commun*. **8**, 14684 (2017).
39. Falanga, V. et al. Full-thickness wounding of the mouse tail as a model for delayed wound healing: accelerated wound closure in *Smad3* knock-out mice. *Wound Repair Regen*. **12**, 320–326 (2004).
40. Rheinwald, J. G. & Green, H. Serial cultivation of strains of human epidermal keratinocytes: the formation of keratinizing colonies from single cells. *Cell* **6**, 331–343 (1975).
41. Nanba, D. et al. Cell motion predicts human epidermal stemness. *J. Cell Biol*. **209**, 305–315 (2015).
42. Inomata, K. et al. Genotoxic stress abrogates renewal of melanocyte stem cells by triggering their differentiation. *Cell* **137**, 1088–1099 (2009).
43. Jonkman, M. F. et al. Revertant mosaicism in epidermolysis bullosa caused by mitotic gene conversion. *Cell* **88**, 543–551 (1997).
44. Pasmooij, A. M., Nijenhuis, M., Brander, R. & Jonkman, M. F. Natural gene therapy may occur in all patients with generalized non-Herlitz junctional epidermolysis bullosa with *COL17A1* mutations. *J. Invest. Dermatol*. **132**, 1374–1383 (2012).
45. Kowalewski, C. et al. Amelioration of junctional epidermolysis bullosa due to exon skipping. *Br. J. Dermatol*. **174**, 1375–1379 (2016).

**Acknowledgements** We thank H. Yokozeki, Y. Nishimori, F. Toki, Y. Kato, M. Fukuda, R. Yajima, A. Tsuda, Y. Muroyama, H. Shimizu, W. Nishie, K. Yancey, T. Usami, F. Ishino and M. Kanai for support, and DASS Manuscript for editing.

E.K.N. is supported by an AMED Project for Elucidating and Controlling Mechanisms of Ageing and Longevity (JP17gm5010002 JP18gm5010002) and a JSPS Grants-in-Aid for Scientific Research S (26221303) and Scientific Research on Innovative Areas “Stem Cell Aging and Disease” (26115003). H. Matsumura is supported by a JSPS Grant-in-Aid for Scientific Research on Innovative Areas “Cell Competition” (26114001).

**Reviewer information** *Nature* thanks Salvador Aznar Benitah, James DeGregori and the other anonymous reviewer(s) for their contribution to the peer review of this work.

**Author contributions** E.K.N. and H. Matsumura conceived the study and wrote the manuscript. N.L. performed the majority of experiments, analysed the data and wrote the manuscript. T.K., D.N. and K.A. analysed human keratinocytes. S.I. performed TEM experiments. A.T. and Y.M. prepared *Epi-Confetti* mice. H. Morinaga performed 8-OHdG staining. T.N. provided human skin specimens. E.G.-L. and A.D.A. provided the *Itga6* floxed mice.

**Competing interests** E.K.N. is an inventor on a patent application (in preparation) related to this manuscript, which will be filed by Tokyo Medical and Dental University.

**Additional information**

**Extended data** is available for this paper at https://doi.org/10.1038/s41586-019-1085-7.
**Supplementary information** is available for this paper at https://doi.org/10.1038/s41586-019-1085-7.
**Reprints and permissions information** is available at http://www.nature.com/reprints.
**Correspondence and requests for materials** should be addressed to H.M. or E.K.N.

## METHODS

**Mice.** C57BL/6N mice were purchased from the Sankyo Laboratory Service. *K14-creERT2* mice[46], *Dct-H2B-GFP* mice[35], *Col17a1* floxed mice[6], *Itga6* floxed mice[47], *K14-human COL17A1* tg mice[33] and *R26R*$^{Brainbow2.1}$ mice[9] have previously been described. All transgenic and mutant mice were backcrossed to C57BL/6J mice obtained from the Sankyo Laboratory Service. Both male and female mice (7 weeks to 30 months old) were used. Mice with asymmetrical wound patches or dyspigmented patches in their tails were not used. The mouse experiments were not randomized and not blinded. No statistical methods were used to predetermine sample size. Mouse care was in accordance with the guidance of the Tokyo Medical and Dental University for mouse and recombinant DNA experiments. All mouse experiments were performed following the Guidelines for the Care and Use of Laboratory Animals and were approved by the Institutional Committee of Laboratory Animals. Offspring were genotyped by PCR-based assays of mouse tail DNA.

**Generation of basal keratinocyte-specific *Col17a1*- and/or *Itga6*-deficient mice.** To delete floxed target gene sequences in basal keratinocytes at specific times, *Col17a1* floxed and/or *Itga6* floxed mice were mated with *K14-creERT2* mice. Mice were treated with 2 mg tamoxifen (TAM) per day for 5 consecutive days at 7 weeks of age by intraperitoneal (i.p.) injection.

**Lineage tracing.** To generate multi-colour labelling in epidermal basal cells from the tail, we generated *K14-creERT2;R26R*$^{Brainbow2.1}$ mice and *Col17a1*$^{fl/fl}$*; K14-creERT2;R26R*$^{Brainbow2.1}$ mice. For long-term clonal tracing, mice were treated with 2 mg TAM per day for 5 consecutive days at 7 weeks of age by i.p. injection. For short-term clonal tracing, mice were treated by i.p. injection with 0.4 mg TAM at 7 weeks of age.

**Human skin specimens.** Tissue specimens of human facial skin were collected from several patients for diagnostic purposes at the Department of Dermatology of the Tokyo Medical and Dental University (TMDU). Those specimens were fixed overnight in 10% formalin solution and then embedded in paraffin. Paraffin sections were deparaffinized, rehydrated and then stained with haematoxylin and eosin (HE). To examine age-associated changes in epidermal thickness in healthy human epidermis, we selected histologically normal skin areas that were not affected by any diseases. More than three specimens of each group from young ($\leq$33 years old) and aged ($\geq$74 years old) tissues were analysed. The use of human skin samples was reviewed and approved in advance by the Ethical Committee of the TMDU. Informed consent including publication of the skin section images was obtained from all tissue sample donors. All relevant ethical regulations on compliance were followed in this study.

**Preparation of paraffin and frozen sections.** For paraffin sections, mouse tail skin specimens were fixed overnight in 10% formalin solution at 4 °C and were then embedded in paraffin. Paraffin-embedded skin specimens were cut into 5-μm-thick sections using a Rotary Microtome HM325 (MICROM International). For frozen sections, mouse tail skin specimens were immersed in ice-cold 4% paraformaldehyde (4% PFA), irradiated in a 500-W microwave oven for three 30-s cycles with intervals and then kept on ice for 20 min. The fixed skin samples were embedded in optimal cutting temperature (OCT) compound (Sakura Finetechnical), snap-frozen in liquid nitrogen and then stored at −80 °C. Frozen samples were cut into 10-μm-thick sections using a CM 1850 cryostat (Leica Microsystems Nussloch).

**Haematoxylin and eosin staining.** Paraffin sections were deparaffinized and then rehydrated. Frozen sections were removed from the OCT compound and then were stained with HE (Sakura Finetechnical).

**Immunofluorescence staining.** Immunofluorescence was performed as previously described[6]. Frozen sections were used for immunofluorescence analysis, except for 8-oxoguanine staining. For p16 (ProteinTech Group) immunostaining, antigen retrieval was performed by boiling the slides for 20 min in Dako target retrieval solution (Dako). Nonspecific staining was blocked by incubation with phosphate-buffered saline (PBS) containing 3% skim milk (Difco) and 0.1% Triton X-100 for 30 min. For immunostaining of DCT, tissue sections were incubated with acetone for 10 min and with methanol containing 0.3% $H_2O_2$ for 30 min for permeabilization. Nonspecific staining then was blocked by incubation with PBS containing 3% skim milk (Difco) and 0.1% Triton X-100 for 30 min. For 8-OHdG immunostaining, paraffin sections were used. Antigen retrieval was performed by boiling the slides for 20 min in Dako target retrieval solution (Dako). Nonspecific staining was blocked by incubation with PBS containing 10% donkey serum and 0.05% Triton X-100 for 30 min. Tissue sections were incubated with the 8-oxoguanine antibody in Dako Fluorescence Mounting Medium (Dako) at 4 °C overnight, and subsequently incubated with secondary antibodies in DAKO Fluorescence Mounting Medium for 2 h at room temperature.

Tissue sections were incubated with the primary antibody at 4 °C overnight and were subsequently incubated with appropriate secondary antibodies conjugated with Alexa Fluor 488, 568, 594 or 680 (Invitrogen-Molecular Probes) for 2 h at room temperature. After washing in PBS, 4′,6-diamidine-2′-phenylindole dihydrochloride (DAPI) (Invitrogen-Molecular Probes) was added for nuclear counterstaining. Coverslips were mounted on glass slides with fluorescent mounting medium (Thermo Electron). All images were obtained using an FV1000 confocal microscope system (Olympus).

**Electron microscopy.** The specimens were fixed in 2% glutaraldehyde and 4% PFA in PBS for 2 h. After washing with PBS, they were immersed in 30% sucrose in PBS and were then embedded in OCT compound (Sakura Finetechnical), snap-frozen in liquid nitrogen and then stored at −80 °C. Frozen samples were cut into 20-μm-thick sections using a CM 1850 cryomicrotome (Leica Microsystems). By adjusting the epidermal orientation using a light microscope, the frozen sections were placed on MAS-coated glass slides (S9441, Matsumani glass). The frozen sections were washed with 0.1 M phosphate buffer, post-fixed in 1% osmium tetroxide in 0.1 M phosphate buffer for 2 h and processed for embedding in Epon-812. Ultrathin sections were prepared and mounted on copper grids, stained with uranyl acetate and lead citrate, and then examined by TEM (H-7100, Hitachi).

**Immunohistochemistry.** For immunohistochemistry staining of COL17A1, human paraffin-embedded sections were deparaffinized and rehydrated. To perform antigen retrieval, sections were microwave heated at 90 °C in target retrieval solution (Dako) for 20 min. Nonspecific staining was then blocked by pre-incubation with PBS containing 0.1% Triton X-100 and 3% skim milk (Difco) for 30 min. Tissue sections were incubated with the COL17A1 antibody (Abcam) at 4 °C overnight, and were subsequently incubated with biotinylated goat anti-rabbit immunoglobulin G antibody (Vector Laboratories) at room temperature for 2 h. After washing, the sections were incubated with avidin-biotin peroxidase complex using the Vectastain Elite ABC kit (Vector Laboratories) at room temperature for 30 min. After colour development with 3,3-diaminobenzidine (DAB) as the substrate, sections were counterstained with haematoxylin. Coverslips were mounted on glass slides with mounting media (Daidosangyo). Images were obtained using an upright BX51 microscope (Olympus).

**Immuno-TEM.** The specimens were immersed in ice-cold 4% PFA in PBS (pH 7.4), irradiated in a 500-W microwave oven for three 30-s cycles with intervals and then kept on ice for 20 min. After washing with PBS, they were immersed in 30% sucrose in PBS and were embedded in OCT compound (Sakura Finetechnical), snap-frozen in liquid nitrogen and then stored at −80 °C. Frozen samples were cut into 20-μm-thick sections using a CM 1850 cryomicrotome (Leica Microsystems). By adjusting the epidermal orientation using a light microscope, the frozen sections were placed on MAS-coated glass slides (S9441, Matsumani glass) on droplets of 1% bovine serum albumin (BSA) and 0.1% saponin in 0.1 M phosphate buffer. The sections were subsequently transferred to droplets of rabbit anti-human COL17A1 (Clone NC16A3, Abcam, diluted 1:20) antibody with 1% BSA and 0.1% saponin in 0.1 M phosphate buffer overnight at 4 °C. Each section was then incubated with 1.4 nm nanogold colloidal particles (Nanoprobes, diluted 1:20) with 1% BSA and 0.1% saponin in 0.1 M phosphate buffer for 2 h. The sections were then washed with 0.1 M phosphate buffer, fixed with 1% glutaraldehyde in 0.1 M phosphate buffer for 10 min and then washed with water. After gold enhancement (Nanoprobes), the sections were washed with water, post-fixed with 1% osmium tetroxide in 0.1 M phosphate buffer, then dehydrated in a graded series of ethanol and embedded in Epon 812. Ultrathin sections were prepared and mounted on copper grids, stained with uranyl acetate and examined using TEM (H-7100, Hitachi).

**Tail epidermal whole-mount immunohistochemistry.** Tissues were processed for tail epidermal whole-mount immunohistochemistry as previously described[48]. In brief, pieces of tail skin were incubated in 5 mM EDTA at 37 °C for 3.5 h to peel the epidermis from the dermis as an intact sheet. Epidermal pieces were fixed in 4% PFA and then stored in 0.1% proclin 150 (Supelco) at 4 °C for up to 3 months before labelling. To verify areas of dyspigmentation in the scale areas, images were acquired using an SVX16 stereo microscope (Olympus). For immunofluorescence staining, epidermal pieces were blocked by incubation in PBS containing 3% skim milk (Difco) and 0.1% Triton X-100 on a shaker for 1 h at room temperature. The samples were incubated with primary antibodies on a shaker for 2 h at room temperature and subsequently incubated at 4 °C overnight. The epidermal pieces were then washed and incubated with appropriate secondary antibodies on a shaker for 2 h. After washing in PBS, DAPI (Invitrogen-Molecular Probes) was added for nuclear counterstaining. Images were acquired using a FV1000 confocal microscope (Olympus).

**Antibodies.** Primary antibodies used included: guinea pig antibody to KRT31 (Progen); rabbit antibody to MCM2 (Abcam); rabbit antibody to COL17A1 (Abcam); rat antibody to ITGA6 (BD Pharmingen); guinea pig antibody to plectin (Progen); rabbit antibody to COL7A1 (Millipore); mouse antibody to ITGB1 (Miltenyi Biotech); rat antibody to ITGB4 (BD Pharmingen); rat antibody to KIT (BD Pharmingen); rat antibody to COL17A1 (Clone 8B6E9, Nishimura laboratory); rat antibody to PH3 (Sigma-Aldrich); rabbit antibody to caspase 3 (Cell Signaling); chicken antibody to GFP (Abcam); mouse antibody to KRT10 (Santa Cruz Biotechnology); rabbit antibody to survivin (Cell Signaling); rat antibody

to PDGFRa (eBioscience); rabbit antibody to phospho-histone H2AX (Cell Signaling); rabbit antibody to DCT (a kind gift from V. Hearing, National Cancer Institute); mouse antibody to 8-OHdG (Abcam); rabbit antibody to p-RPA2/32 (Abcam).

Secondary antibodies used included: Alexa Fluor 488 donkey antibody to rat immunoglobulin (IgG) (Invitrogen-Molecular Probes); Alexa Fluor 488 donkey antibody to mouse IgG (Molecular Probes); Alexa Fluor 488 donkey antibody to chicken IgY (Jackson Immuno Research Laboratories); Alexa Fluor 568 goat antibody to guinea pig IgG (Molecular Probes); Alexa Fluor 594 donkey antibody to goat IgG (Molecular Probes); Alexa Fluor 594 donkey antibody to rat IgG (Jackson); Alexa Fluor 594 donkey antibody to rabbit IgG (Molecular Probes); Dylight 594 donkey antibody to mouse IgG (Jackson); Alexa Fluor 680 donkey antibody to rabbit IgG (Molecular Probes); biotinylated goat anti-rabbit immunoglobulin G antibody (Vector Laboratories).

**Measurements.** To measure the thickness of mouse and human epidermis, the paraffin and frozen sections were stained with HE. Images were acquired using an upright BX51 microscope (Olympus). In mouse epidermis, the thickness was measured as the distance from the basal to the spinous layer in the middle of the tail scale region. In human epidermis, the average human epidermal thickness was obtained by measuring the epidermal area (basal layer to granular layer) and the length of the granular layer using ImageJ.

To count the epidermal layers, tail sections were stained with KRT31. The $KRT31^+$ layers containing $DAPI^+$ cells were then counted.

To count the total basal cells and $MCM2^+$ basal cells, tail sections were stained for MCM2, after which the total basal cells and $MCM2^+$ basal cells were counted.

To count hemidesmosomes and micro-delaminations, >5 TEM images at ×20,000 magnification were acquired at sites of the basement membrane of the tail scale area from each specimen. The numbers of hemidesmosomes with or without micro-delaminations and basement-membrane length were measured using ImageJ. The numbers of hemidesmosomes per μm or micro-delaminations per μm were then calculated.

To measure the $COL17A1^+$ immuno-gold colloid, the number of gold colloidal particles along hemidesmosomes and basement-membrane length was counted using ImageJ. The number of gold colloid particles per μm was then calculated.

To measure the expression levels of hemidesmosomes and basement-membrane components, immunofluorescence images of slides immunostained for COL17A1, ITGA6, plectin, COL7A1, ITGB4 and ITGB1 were acquired. Fluorescent intensities were measured using ImageJ following background removal and normalization with DAPI.

To measure the expression levels of COL17A1 in human skin epidermis, human facial skin specimens were stained immunohistochemically for COL17A1. Colour development was performed using 0.05% DAB. HE and DAB stained images were acquired using an upright BX51 microscope (Olympus). DAB intensity was measured using ImageJ Fiji by colour deconvolution with the removal of the background colour and normalization by haematoxylin.

To measure single-colour-marked clones from *K14-creERT2;R26R*$^{Brainbow2.1}$ or *Col17a1*$^{fl/fl}$*;K14-creERT2;R26R*$^{Brainbow2.1}$ mice, tail whole-mount images were acquired using an FV1000 confocal microscope (Olympus). The size and number of $RFP^+$ single clones were then measured using ImageJ.

To measure the correlation between COL17A1 expression and sizes of single-colour clones in *K14-creERT2;R26R*$^{Brainbow2.1}$ mice, tail sections were stained for COL17A1. The fluorescent intensity of COL17A1 and the size of $RFP^+$ or $GFP^+$ single clones were then measured using ImageJ.

To count single-colour-marked basal and floating clones from *K14-creERT2;R26R*$^{Brainbow2.1}$, *Col17a1*$^{fl/+}$*;K14-creERT2;R26R*$^{Brainbow2.1}$ and *Col17a1*$^{fl/fl}$*;K14-creERT2;R26R*$^{Brainbow2.1}$ mice, tail sections were stained for COL17A1 2 and 28 days after TAM treatment. The number of basal and floating clones were counted, then the percentage was calculated.

To measure single-colour-marked delamination clones in floating clones from *K14-creERT2;R26R*$^{Brainbow2.1}$ and *Col17a1*$^{fl/fl}$*;K14-creERT2;R26R*$^{Brainbow2.1}$ mice, tail sections were stained with KRT31 28 days after TAM treatment. The different types (single or multiple) of floating clones in the $KRT31^+$ scale area were counted, then the percentage of clones per scale was calculated.

To count caspase 3 $(CASP3)^+$ cells, tail sections and the positive control (dorsal skin 1 day after 10 Gy irradiation) were stained for COL17A1 and CASP3. $CASP3^+$ cells in the basal layers were counted as apoptotic cells.

To measure levels of $p16^+$, tail sections and the positive control (DMBA/TPA-induced papilloma) were stained for p16. $p16^+$ cells in the basal layers were counted as senescent cells.

To measure levels of $MCM2^+$ from *K14-creERT2;R26R*$^{Brainbow2.1}$ and *Col17a1*$^{fl/fl}$*;K14-creERT2;R26R*$^{Brainbow2.1}$ mice, tail sections were stained for MCM2 28 days after TAM treatment. The fluorescent intensity of single-colour-marked basal cells was measured using ImageJ by background removal and normalization with DAPI.

To measure levels of COL17A1 in $\gamma$-$H2AX^{high/mean}$ cells from aged tail skin, tail sections were stained for COL17A1 and γ-H2AX. The fluorescent intensity of COL17A1 in $\gamma$-$H2AX^{high}$ or $\gamma$-$H2AX^{mean}$ cells was measured using ImageJ by background removal and normalized with DAPI.

To count epidermal melanoblasts or melanocytes in aged mice and in *Col17a1*- or *Itga6*-deficient mice, tail sections and whole-mount specimens were stained for KRT31 and/or KIT. In aged mice, the numbers of $KIT^+$ cells from wild-type mice and $GFP^+$ cells from *Dct-H2B-GFP* tg mice in the $KRT31^+$ scale area were counted. In *Col17a1*- or *Itga6*-deficient mice, the numbers of $GFP^+$ cells from *Dct-H2B-GFP* tg mice in the scale area with or without melanin were counted.

To count $PDGFRa^+$ mesenchyme cells, tail sections were stained for PDGFRa. $PDGFRa^+$ cells directly beneath the basement membrane were counted.

To measure the cell division angle, frozen sections of tail skin were stained for COL17A1 and survivin. Cell spindle orientation was determined by the angle between survivin, which accumulates in the mid-body, and COL17A1 at the basement membrane during telophase. For all experiments, at least three randomized different scales in each sample (indicated in each legend) were counted.

**Cell lines.** HaCaT cells (ATCC) or normal human epidermal keratinocytes (NHEKs) (Kurabo) which were authenticated by the vendor were used in this study. The cells were routinely tested by the venders and found to be negative for mycoplasma infection. The cell line experiments were not randomized and not blinded. No statistical methods were used to predetermine sample size.

**Cycloheximide (CHX) pulse chase assay.** To inhibit new synthesis of proteins, NHEKs were incubated with 10 μM CHX (Wako) for 1, 3, 6, 12 or 24 h before collecting. Keratinocytes were grown for seven days in culture before the experiment. After the removal of 3T3 feeder cells by gentle pipetting, keratinocytes were then subjected to western blotting analysis. For combined treatment with marimastat, a pan-metalloproteinase inhibitor, lysates of NHEKs were collected 0, 7 and 24 h after treatment with 3 μM marimastat with or without CHX.

**Flow cytometry and cell sorting.** NHEKs were grown for seven days in culture and trypsinized before the experiments. Resuspended keratinocytes were then incubated with a rabbit monoclonal antibody against COL17A1 (1:50, Abcam) for 1 h on ice and washed with 2% fetal bovine serum (FBS) in PBS. Subsequently, the cells were incubated with an Alexa Fluor 488-conjugated rabbit polyclonal antibody (1:50, Molecular Probes) or normal rabbit IgG (1:50, Santa Cruz Biotechnology) for 1 h on ice. After being washed with 2% FBS in PBS, cells were resuspended in culture medium. Cells were then collected using FACSAria IIIu (BD) and subjected to colony-formation assay.

**Western blotting.** NHEKs and HaCaT keratinocytes were collected, homogenized and sonicated in TNE buffer (10 mM Tris-HCl, pH 7.5, 150 mM NaCl and 1 mM EDTA) containing 1× protease inhibitor tablet (Roche), 1× phosphatase inhibitor tablet (Roche) and 1% NP-40. Protein concentrations were measured using a BCA Protein Assay Kit (Pierce). The cell lysates were subjected to mini-protean-tgx-precast gel (Bio-Rad) electrophoresis (0.02 mA/mini-gel) for 1 h. The gels were then transferred to PVDF membranes for 1 h at 90 V or 1 h at 250 mA using a mini transblot cell (Bio-Rad). The membranes were then immersed in Blocking One (Nacalai Tesque) for 30 min and then incubated overnight with each primary antibody diluted in Blocking One. Primary antibodies used included: a mouse monoclonal antibody to human COL17A1 (Clone NC16A3, 1:100), a mouse monoclonal antibody against plectin (1:200, Cosmo Bio), a rabbit polyclonal antibody against ITGA6 (1:1,000, Abcam), a rabbit polyclonal antibody against ITGB4 (1:1,000, Santa Cruz Biotechnology), a rabbit monoclonal antibody against ITGB1 (1:2,000, Abcam), a rabbit monoclonal antibody to phospho-histone H2AX (1:1,000, Cell Signaling), a rabbit polyclonal antibody to αβ-tubulin (1:500, Cell Signaling, Beverly, MA, USA), a rabbit monoclonal antibody against GAPDH (1:5,000, Cell Signaling) and a mouse monoclonal antibody against β-actin (1:15,000, Sigma). After being washed three times for 5 min each with 1× TBST (25 mM Tris-HCl, pH 7.4, 150 mM NaCl, 0.1% Tween-20), the membranes were incubated for 2 h with horseradish peroxidase (HRP)-conjugated secondary antibodies against mouse IgG (GE healthcare, Port Washington, NY, USA) or rabbit IgG (GE healthcare) and washed three times for 5 min each with 1× TBST. After incubation with a Luminata Forte Western HRP Substrate detection system (Millipore) for a few minutes, immunoblot images were acquired using an LAS-3000 luminescence image analyser (Fuji Photo film, Tokyo, Japan) or a Fusion FX6 System (Vilber lourmat).

**Transfection of small interfering RNAs into human epidermal keratinocytes.** NHEKs were maintained in Dermalife K Medium Complete kit (Kurabo) at 37 °C. To transduce small interfering (si)RNAs into keratinocytes, each siRNA was transfected with Lipofectamine RNAiMAX reagent (Invitrogen) according to the manufacturer's instructions with modifications. In brief, keratinocytes were plated in 6-well plates at a density of 100,000 cells per well and incubated for 2 h. To prepare the RNAiMAX liposome solution with siRNA, 2 μl RNAiMAX and 2 μl 10 μM siRNA were gently mixed into 500 μl Opti-MEM solution (GibcoBRL) and incubated for 15 min at room temperature. After incubation, the RNAiMAX liposome solution was added to the cells in the six-well plates. The cells were then subjected

to immunostaining or western blotting analysis. siRNAs used in this study were named as follows: siRNA-controlB, siRNA-COL17A1 and siRNA-ITGA6 (Santa Cruz Biotechnology).

**UVB irradiation in vivo and in vitro.** To stabilize the dose of UVB emission, the UVB irradiation machine (YAYOI) was pre-warmed for 10 min. The dose of UVB emission was measured with a UV photometer. Seven-week-old C57BL/6N mice were exposed to UVB (200 mJ/cm$^2$) irradiation, once daily for five consecutive days for four weeks in a mouse cage bottom covered with a transparent polyester garbage bag. For immunohistochemical analysis, tails were biopsied four days after the final UVB exposure. For western-blot analysis, HaCaT cells or NHEKs were plated in 6-well plates at a density of 250,000 cells per well and were then irradiated by UVB in a plastic dish. HaCaT cells were collected 24 h after the 20 or 40 mJ/cm$^2$ UVB exposure. NHEKs were collected 12 h after 0, 40 or 80 mJ/cm$^2$ UVB irradiation with or without 3 μM marimastat treatment.

**Ionizing radiation in vitro.** HaCaT cells were plated into 6-well plates at a density of 250,000 cells per well and incubated for 24 h. The culture medium was replaced by Dulbecco's modified Eagle's medium (DMEM), then low-pressure irradiation of cells was performed using an RX-650 (Faxitron X-ray) at 100 kVp without filter (dose rate ∼3 Gy/min). Cells were collected 72 h after 20–30 Gy ionizing radiation treatment.

**Hydrogen peroxide treatment in vitro.** HaCaT cells were plated into 6-well plates at a density of 100,000 cells per well and incubated for 24 h. The cells were then cultured for 24 h in DMEM containing 250 μM hydrogen peroxide (Nacalai Tesque). Cells were collected 24 h after treatment.

**Hydroxyurea (HU) treatment in vivo.** To treat cells with HU in vivo, 7-week-old wild-type mice were injected i.p. with 100 μl HU (25 mg/ml) for 4 consecutive days or for 3 consecutive days per week for 3 weeks. Samples were collected 2 h after the last HU treatment.

**Plasmids.** To generate the pCMV-EmGFP-miR-COL17A1 vector, more than two sets of synthetic oligonucleotides for each gene were obtained from the Life Technology custom primer website (https://rnaidesigner.thermofisher.com/rnaiexpress/rnaiExpress.jsp) (designed by Block-it miR RNAi technology, Life Technology). The double-stranded DNA of each gene was inserted into 5′-miR and 3′-miR flanking sequences of the pcDNA6.2-GW/EmGFP-miR plasmid (Life Technology). To select effective knockdown vectors for each gene, we transfected them into HaCaT cells and validated them. Effective primers sequences used in this study are as follows: miR-COL17A1 F, TGCTGAA TACTGTCACTCTGCATGTAGTTTTGGCCACTGACTGACTACATGCAGTG ACAGTATT; miR-COL17A1 R, CCTGAATACTGTCACTGCATGTAGTCAGTC AGTGGCCAAAACTACATGCAGAGTGACAGTATTC.

**Generation of stable HaCaT cell lines.** Before gene transduction, HaCaT cells were maintained in DMEM (Gibco) supplemented with 10% (v/v) FBS at 37 °C. To obtain stable mutant cells, *pCMV-EmGFP-miR-SCRAMBLE* (pcDNA6.2-GW/EmGFP-miR neg control) and *pCMV-EmGFP-miR-COL17A1* were transfected into HaCaT cells with Fugene hemidesmosome reagent (Promega) according to the manufacturer's instructions. The cells were then selected with 5 μg/ml blasticidin S solution (Wako) for 14 days. GFP$^{high}$ population cells were sorted out using a FACS aria II (BD Bioscience). HaCaT stable cell lines were subjected to 3D culture.

**Three-dimensional cultures of HaCaT cells.** To perform 3D cultures of HaCaT cells, we used the LabCyte EPI-MODEL (J-TEC). In brief, cell culture inserts (0.4-μm pore size, PET track-etched membrane, Corning) were transferred into 12-well culture dishes and filled with 1 ml 3D differentiation medium (J-TEC). HaCaT cells were then cultured on the culture inserts at a density of 250,000 cells per well in 5% $CO_2$ at 37 °C. After 1 day of incubation, the residual medium inside each culture insert was removed to expose the cells to air. To maintain the 3D culture, the 3D differentiation medium outside each culture insert was changed every 3 days. After culture for 14 days, 3D cultured tissue samples were collected. For cell competition assays, GFP$^+$ mutant HaCaT cells were mixed with wild-type HaCaT cells at ratios of 1:0, 1:3 and 1:10.

**Colony-forming assays using mouse tail epidermis.** 3T3-J2 fibroblasts, originally provided by H. Green (Harvard Medical School) were treated with mitomycin-C and seeded at a density of 200,000 cells per well into 6-well culture plates in DMEM containing 10% FBS and 1% antibiotics (penicillin/streptomycin/amphotericin B) (Wako). To allow cells to attach to the dishes, the mitomycin-C treated 3T3-J2 fibroblasts were cultured for 24 h in 5% $CO_2$ at 37 °C. For colony-forming assays, epidermal keratinocytes from mouse tail skin were prepared as previously described[8]. In brief, epidermal sheets were prepared by placing small pieces in 2 mg/ml dispase solution (Invitrogen) at 37 °C for 30 min. After incubation, the epidermis was gently teased from the dermis as an intact sheet. The epidermis was minced and dissociated by treatment with 0.25% trypsin solution (Gibco-Invitrogen) for 10 min at room temperature. To inactivate the trypsin activity, keratinocytes were suspended with 1× PBS containing 20% FBS. To obtain dissociated keratinocytes, keratinocytes were filtered through a 40-μm cell strainer. The dissociated keratinocytes were seeded onto 3T3-J2 feeder cells at a density of 400–2,000 cells per well in 6-well culture dishes in DMEM/Ham's F-12 medium (3:1), supplemented with $1.8 \times 10^{-4}$ M adenine, $3.1 \times 10^{-4}$ M L-glutamine (Gibco), 5 μg/ml hydrocortisone, 5 μg/ml insulin, $10^{-9}$ M cholera enterotoxin, 100 ng/ml EGF, 10% FBS and 1% antibiotics solution (Wako) at 32 °C in a humidified atmosphere with 8% $CO_2$ and 5% $O_2$ for 12 days. To visualize the keratinocyte colonies, the cells were fixed in 10% formalin for 25 min at room temperature, after which the colony-containing dishes were stained with crystal violet for 5 min at room temperature. The numbers of all colonies and colonies with a diameter larger than 0.5 mm were counted.

**Microarray analysis.** To analyse global gene expression changes during ageing in total tail IFE, specimens of total tail IFE were collected from young and aged mice. Microarray analysis was performed as previously described[6]. In brief, the total IFE was collected by treatment with 5 mM EDTA for 3–3.5 h. After gentle mincing, samples were placed into lysis solution with 2-ME (mercaptoethanol) (Sigma). After mixing the lysis solution using a bead crusher, μT-01 (TAITEC), total RNAs were isolated using a GenElute mammalian Total RNA miniprep Kit (Sigma) according to the manufacturer's instructions. RNAs were labelled with cyanine 3 (Cy3) using a LowInput Quick AMP Labelling Kit (Agilent Technologies) according to the manufacturer's instructions. Cy3-labelled cRNA was prepared from 0.1 μg RNA and the cRNA quality and cyanine incorporation were analysed using an Agilent Bioanalyzer 2100 (Agilent) and a Nanodrop ND-1000 Spectrophotometer (Thermo Fisher Scientific). For each hybridization, 0.6 μg Cy3-labelled cRNA was fragmented and hybridized at 65 °C for 17 h to an Agilent SurePrint G3 Mouse GE 8 × 60K Microarray (design ID 028005). After washing, microarrays were scanned using an Agilent DNA microarray scanner (G2600D). For normalization of microarray data, the intensity value of each scanned feature was quantified using Agilent feature extraction software version 11.5.1.1, which performs background subtractions. We only used features that were flagged as no errors (detected flags) and excluded features that were not positive, not significant, not uniform, not above background, saturated or population outliers (compromised and not detected flags). Normalization was performed as (per chip: normalization to 75 percentile shift; per gene: normalization to median of all samples). There are 24,321 Entrez gene RNAs and 4,576 long non-coding RNAs on the Agilent SurePrint G3 Mouse GE 8 × 60K Microarray (design ID 028005) without control probes. Altered transcripts were quantified using the comparative method. We applied more than a twofold change in signal intensity to identify significant differences of gene expression in this study.

**Gene Ontology analysis using MeV and DAVID software.** To generate the gene expression comparison data as a heat map, TIGRMeV software (version 4.8.1, http://mev.tm4.org/#/welcome) was used. To analyse Gene Ontology (GO) terms of ≥2.0-fold increased or decreased gene clusters, the web-based (https://david.ncifcrf.gov/) Database for Annotation, Visualization and Integrated Discovery (DAVID) 6.7 was used. To extract reliable GO terms belonging to biological processes, we used Fisher's exact test and multiple test correction ($P < 0.05$).

**Full thickness wounding of tail epidermis.** Before surgery, mice were anaesthetized using an avertin solution (1.25% 2,2,2-tribromoethanol and 2.5% 2-methyl-2-butanol, Sigma). A full-thickness wound 10 mm × 3 mm (length × width) was created on the dorsal aspect of each tail, 10 mm distal to the mouse's body, using a scalpel. Haemostasis of the wound area was performed by simple application of pressure to the wound, then each wound was covered with a film spray dressing (Cavilon, 3M). To measure the un-repaired wound area following creation of the full-thickness wound, tail-wound images were taken every week using a digital camera. Wound areas were measured using ImageJ.

**In vitro assessment of chemical inducers of COL17A1.** To identify chemical compounds that induce COL17A1 expression, we selected candidate chemicals that potentially increased the stem cell property or reduced production of reactive oxygen species based on in silico information. To assess the effects of candidate chemical inducers of COL17A1 by western blotting, we seeded 100,000 HaCaT human keratinocytes into 6-well tissue culture plates and then treated them with vehicle (DMSO), 1–60 μM apocynin (Toronto Research Chemicals) or 1–10 μM Y-27632 (Wako) for 24 h. Cells were collected, homogenized and sonicated in TNE buffer containing 1× protease inhibitor tablet (Roche) and 1× phosphatase inhibitor tablet (Roche). These lysates were then subjected to western blot analysis as described above. To quantify the induction of COL17A1 expression, we performed band lane analysis to determine the ratio of COL17A1 (180 kDa) relative to GAPDH protein levels compared to the control using an LAS-3000 luminescence image analyser (Fuji Photo film) or a Fusion FX6 System (Vilber lourmat).

**Colony-formation assays using human epidermal keratinocytes.** NHEKs were maintained in Dermalife K Medium Complete KIT (Kurabo) at 37 °C. Cells were cultivated in 6-well plates at 200 cells/well on a feeder layer of irradiated or mitomycin C–treated 3T3-J2 cells, at 37 °C and 10% $CO_2$ in a 3:1 mixture of DMEM and Ham's F12 medium supplemented with 10% FBS, 5 μg/ml insulin, 0.4 μg/ml hydrocortisone, $10^{-10}$ M cholera toxin and $2 \times 10^{-9}$ M triiodothyronine,

as previously described[9]. Keratinocytes were cultured for 12 days in the presence or absence of apocynin (10 μM) or Y-27632 (10 μM). The medium was changed every 4 days. Cultures were fixed with 3.7% buffered formaldehyde and stained with 1% rhodamine B, after which keratinocyte colonies were counted using a SMZ645 binocular microscope (Nikon). The numbers of all colonies and colonies with a diameter >2 mm were counted. The areas of colonies were calculated using ImageJ, and the average area of the five largest colonies was acquired.

**In vivo assessment of COL17A1 inducers at wound areas.** To administer drugs at wound areas, we generated full thickness wounds as described above and the wound edge areas were treated with 20 μl vehicle (0.5% DMSO in PBS), 20 μM Y-27632 (in 0.5% DMSO in PBS) or 100 μM apocynin (0.5% DMSO in PBS). After wound creation, the drugs were administered for five consecutive days per week for two weeks. To evaluate drug effects, the percentage of wound areas remaining was calculated using ImageJ. To confirm reproducibility, we repeatedly performed similar experiments at least three times with independent investigators.

**Statistical analysis.** PRISM6 software (Graph Pad Software) or Excel (Microsoft) were used to assess statistical significance. To determine significance between two groups, comparisons were performed using an unpaired two-tailed Student *t*-test or Mann–Whitney *U*-test. For multiple comparisons, one-way ANOVA with Dunnett's or Tukey–Kramer post hoc test or Kruskal–Wallis test with Dunn's post hoc test were performed. $P < 0.05$ was considered statistically significant.

**Reporting summary.** Further information on research design is available in the Nature Research Reporting Summary linked to this paper.

## Data availability

Microarray data were deposited in Gene Expression Omnibus under series identifier GSE111825. All other data that support the conclusions are available from the authors on request.


46. Vasioukhin, V., Degenstein, L., Wise, B. & Fuchs, E. The magical touch: genome targeting in epidermal stem cells induced by tamoxifen application to mouse skin. *Proc. Natl Acad. Sci. USA* **96**, 8551–8556 (1999).
47. Niculescu, C. et al. Conditional ablation of integrin alpha-6 in mouse epidermis leads to skin fragility and inflammation. *Eur. J. Cell Biol.* **90**, 270–277 (2011).
48. Braun, K. M. et al. Manipulation of stem cell proliferation and lineage commitment: visualisation of label-retaining cells in wholemounts of mouse epidermis. *Development* **130**, 5241–5255 (2003).

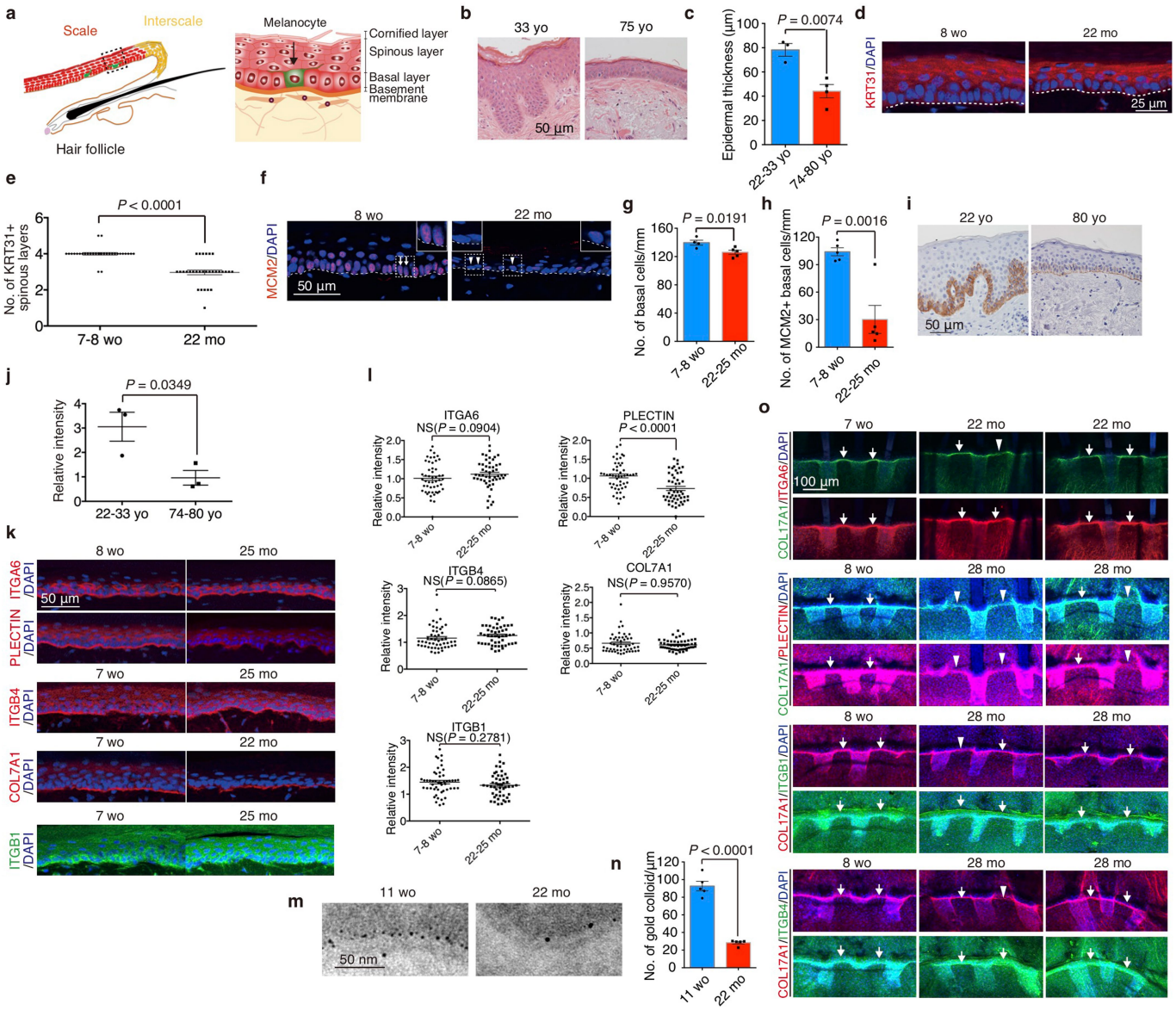


**Extended Data Fig. 1 | Chronological ageing induces the instability of hemidesmosome components. a**, Left, schematic of a scale (red) and interscale (yellow) area of mouse tail epidermis. Right, schematic of a magnified view of the scale, which consists of well-stratified keratinocyte layers that contain epidermal melanocytes or melanoblasts (green) in the basal layer and dermal fibroblasts (orange) in the dermis. **b**, **c**, Representative HE images (**b**) and quantification of epidermal thickness (**c**) of facial skin from young (22–33-year-old, $n = 3$) and aged (74–80-year-old, $n = 4$) humans. Human epidermal thickness was significantly decreased by ageing. **d**, Representative immunofluorescence images of KRT31 in tail scale IFE in young (8 wo) and aged (22 mo) mice. Dashed lines, basement membrane. **e**, Quantification of the number of KRT31$^+$ spinous layers in tail scale IFE from young (7–8 wo, $n = 30$ scales) and aged (22 mo, $n = 30$) wild-type mice. KRT31$^+$ spinous cell layers in the tail scale IFE were decreased by ageing. **f**, Representative immunofluorescence images of MCM2$^+$ (non-$G_0$) cells in tail scale IFE from 8 wo and 22 mo wild-type mice. Basal cells in young tail skin show a perpendicularly polarized structure against the basement membrane (arrows), whereas basal cells in aged tail skin usually show a flattened structure (arrowheads). Small insets, magnified views of dashed boxes. **g**, **h**, Numbers of DAPI$^+$ basal cells (**g**) and MCM2$^+$ basal cells at the non-$G_0$ state (**h**) in tail scale IFE from young (7–8 wo, $n = 4$ in **f**, $n = 5$ in **g**) and aged (22–25 mo, $n = 5$) wild-type mice. **i**, **j**, Representative immunohistochemical images (**i**) and quantification of COL17A1$^+$ DAB signals (**j**) in facial skin from young (22–33-year-old, $n = 3$) and aged (74–80-year-old, $n = 3$) humans. COL17A1 expression was significantly decreased by ageing. **k**, **l**, Representative immunofluorescence images and fluorescent intensities of hemidesmosome and basement membrane components, ITGA6, plectin, ITGB4, COL7A1 and ITGB1 in tail scale areas from young (7–8 wo, $n = 50$ scales) and aged (22–25 mo, $n = 50$) mice. **m**, Representative ultrastructural images of COL17A1 immunogold signals at the basement membrane in young (11 wo) and aged (22 mo) mice. **n**, Quantification of COL17A1$^+$ immunogold particles on the basement membrane in young (11 wo, $n = 5$ hemidesmosomes) and aged (22 mo, $n = 5$) mice. COL17A1$^+$ immunogold signals at the basement membrane were significantly decreased by ageing. **o**, Representative whole-mount immunofluorescence images of COL17A1/ITGA6, COL17A1/plectin, COL17A1/ITGB4 and COL17A1/ITGB1 expression in tail skin from young (7–8 wo) and aged (22–28 mo) mice. Similar results were obtained in at least two independent experiments. Arrows, intact expression; arrowheads, decreased expression. Heterogeneous destabilization of COL17A1 (arrowheads) was stochastically observed in the aged IFE. Mean ± s.e.m.; two-tailed Mann–Whitney *U*-test (**e**, **l**) or two-tailed *t*-test (**c**, **g**, **h**, **j**, **n**).

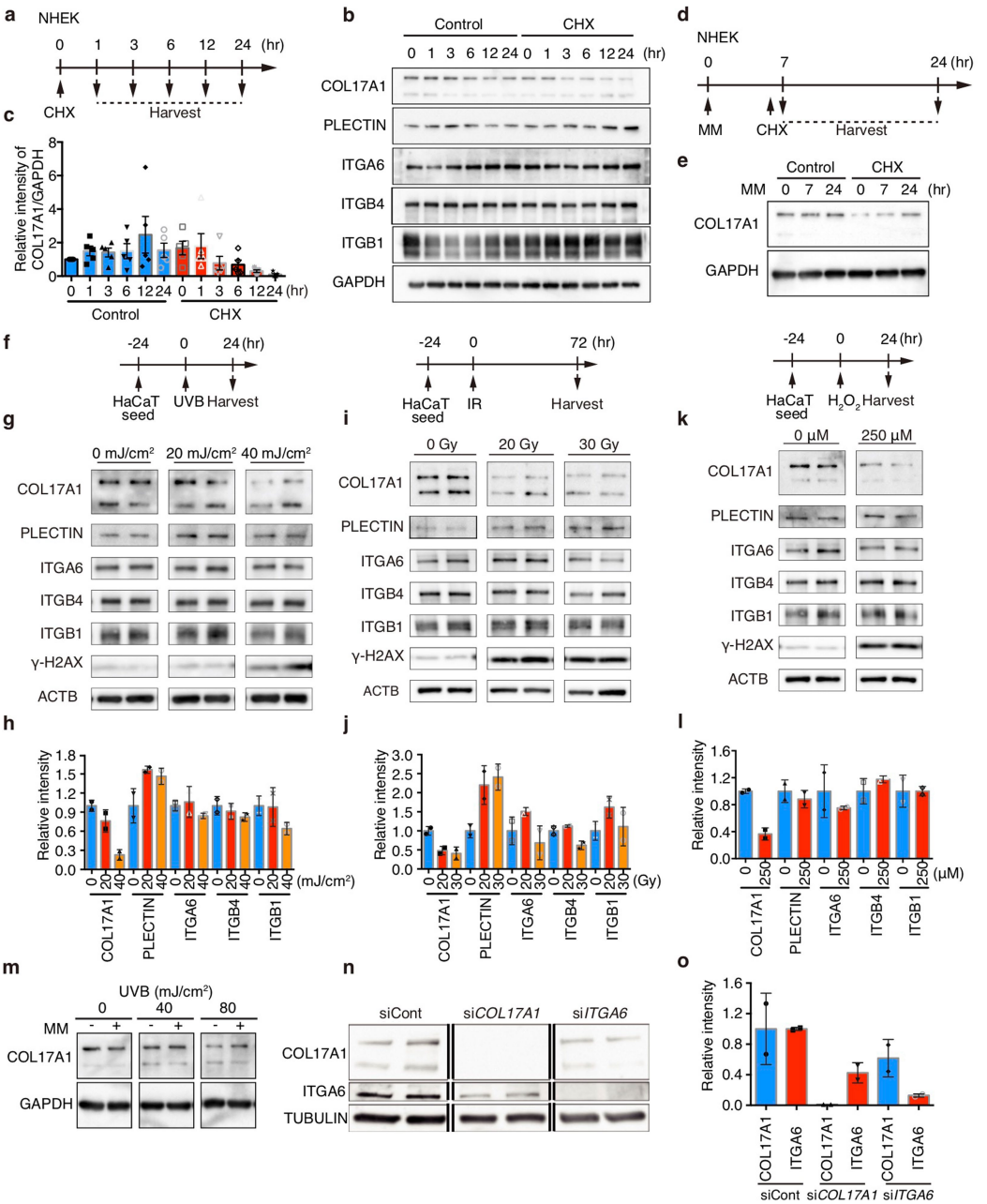


**Extended Data Fig. 2 | COL17A1 is the most unstable hemidesmosome component under genotoxic stress. a**, **d**, Experimental design of the CHX chase assay. Lysates of NHEKs were collected 0, 1, 3, 6, 12 or 24 h after treatment with or without 10 μM CHX (**a**) or 0, 7 or 24 h after treatment with 3 μM marimastat (MM) with or without CHX (**d**). **b**, Western blot analysis of COL17A1, plectin, ITGA6, ITGB4, ITGB1 and GAPDH in NHEKs after CHX treatment for 0, 1, 3, 6, 12 or 24 h. Only COL17A1 showed protein degradation from 6 h; other hemidesmosome components were more stable. Data are representative of at least two independent experiments. **c**, Quantification of band intensities of COL17A1 relative to GAPDH ($n = 5$). **e**, Western blot analysis of COL17A1 and GAPDH in NHEKs after marimastat treatment with or without CHX. Marimastat partially rescued the CHX-induced decrease in COL17A1 expression. Data are representative of at least three independent experiments. **f**, Experimental design for western blot analysis of hemidesmosome components in HaCaT keratinocytes. Cells were seeded 24 h before stress treatments. Cell lysates were collected 24 h after UVB or $H_2O_2$ treatment and 72 h after ionizing radiation. **g**, **i**, **k**, Western blot analysis of COL17A1, plectin, ITGA6, ITGB4, ITGB1, γ-H2AX and β-actin (ACTB) in HaCaT cells with or without 20 or 40 mJ $cm^{-2}$ UVB irradiation (**g**), 20 or 30 Gy ionizing radiation (**i**), and 250 μM $H_2O_2$ (**k**). **h**, **j**, **l**, Band intensities of hemidesmosome components and ITGB1 relative to ACTB ($n = 2$). **m**, Cell lysates of NHEKs were collected 12 h after 0, 40 or 80 mJ $cm^{-2}$ UVB with or without 3 μM marimastat. Marimastat treatment partially rescued UVB-induced COL17A1 destabilization. **n**, Western blot analysis of COL17A1 and ITGA6 in NHEKs after transfection with scrambled siRNA (siCont), *COL17A1* siRNA (si*COL17A1*) or *ITGA6* siRNA (si*ITGA6*) for 72 h. Data are representative of at least two independent experiments. **o**, Band intensities of COL17A1 or ITGA6 relative to tubulin in **n** ($n = 2$). *COL17A1* knockdown destabilizes ITGA6, whereas *ITGA6* knockdown destabilizes COL17A1. Mean ± s.d. (**c**, **h**, **j**, **l**, **o**).

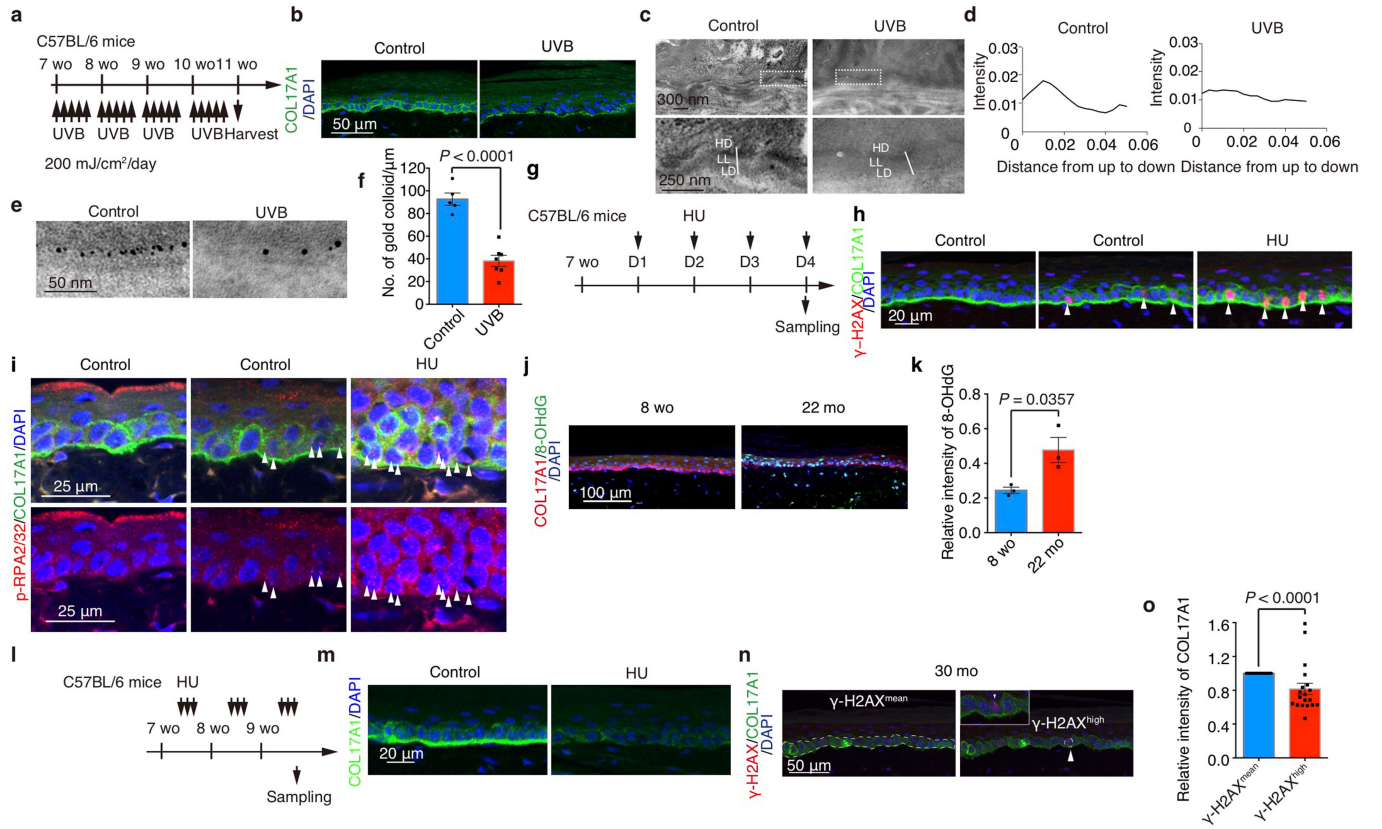


**Extended Data Fig. 3 | The DNA damage response underlies age-associated proteolysis of COL17A1 in vivo. a**, Experimental design. Wild-type mice were exposed to UVB at a dose of 200 mJ $cm^{-2}$, once daily for 5 consecutive days every week from 7 wo to 11 wo, and skin samples were collected 4 days after the last UVB irradiation. **b**, Representative immunofluorescence images of COL17A1 in the scale IFE in control and UVB-irradiated mice. UVB irradiation led to a linearized loss of the COL17A1 expression pattern. Data are representative of at least two independent experiments. **c**, Representative ultrastructural images of epidermal basal cells from control (11 wo, $n = 3$) and UVB-irradiated (11 wo, $n = 3$) mice assessed by TEM. Bottom, enlarged views of the dashed boxed areas in top panels; white lines show regions across the hemidesmosome, lamina lucida and lamina densa. **d**, Intensity histogram (above lines) for hemidesmosomes. UVB irradiation led to the loss of hemidesmosome density. **e**, Representative ultrastructural images of $COL17A1^+$ immunogold signals at the basement membrane in control (11 wo) and UVB-irradiated (11 wo) mice. **f**, Numbers of $COL17A1^+$ immunogold particles at the basement membrane in control (11 wo, $n = 5$ hemidesmosomes) and UVB-irradiated (11 wo, $n = 7$ hemidesmosomes) mice. $COL17A1^+$ immunogold signals at the basement membrane were significantly decreased by UVB irradiation. **g**, **l**, Experimental designs. Seven-week-old wild-type mice were intraperitoneally injected with 100 μl HU (25 mg $ml^{-1}$) for 4 consecutive days (**g**) or for 3 consecutive days per week for 3 weeks (**l**). Samples were collected 2 h (**g**, **l**) after the final HU treatment. **h**, **i**, Representative immunofluorescence images of COL17A1 and γ-H2AX (**h**) or p-RPA2/32 (**i**) 4 days after HU treatment. γ-H2AX foci and p-RPA2/32 foci (arrowheads) were both occasionally found in young tail scale basal cells and were significantly increased by HU treatment. Similar results were obtained in at least two independent experiments. **j**, Representative immunofluorescence images of COL17A1 and 8-OHdG in young (8 wo) and aged (22 mo) scale IFE. Accumulation of 8-OHdG-retaining basal cells and loss of COL17A1 expression were observed in the aged tail skin. **k**, 8-OHdG intensity in tail basal scale cells from young (8 wo, $n = 3$) and aged (22 wo, $n = 3$) mice. **m**, Representative immunofluorescence images of COL17A1 three weeks after HU treatment. Reduced COL17A1 expression was observed three weeks after HU treatment. Similar results were obtained in at least two independent experiments. **n**, Representative immunofluorescence images of COL17A1 and γ-H2AX in aged (30 mo) scale IFE. **o**, COL17A1 intensity in $\gamma\text{-H2AX}^{high}$ (arrowhead in **n**) and $\gamma\text{-H2AX}^{mean}$ (average level) cells from tail basal scale IFE from aged (22–30 mo, $n = 19$ scales) mice. $\gamma\text{-H2AX}^{high}$ cells contain significantly less COL17A1 than $\gamma\text{-H2AX}^{mean}$ cells. Mean ± s.e.m. (**f**, **k**, **o**); two-tailed Mann–Whitney *U*-test (**o**) or two-tailed *t*-test (**f**, **k**).

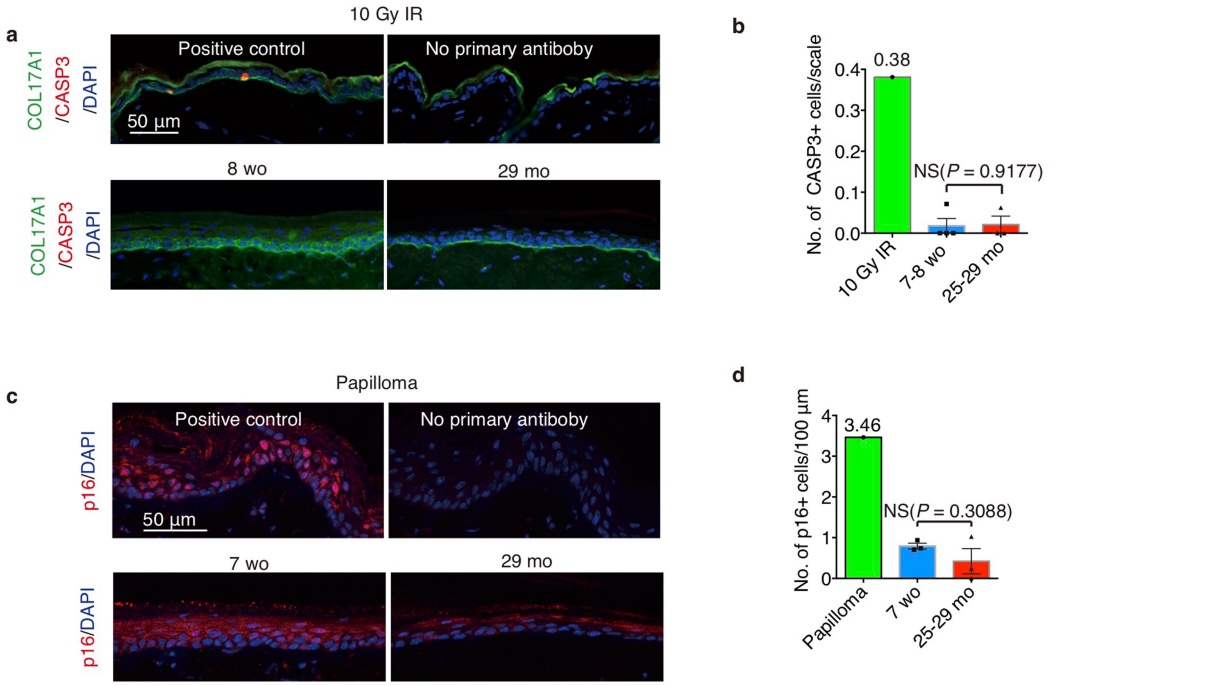


**Extended Data Fig. 4 | There is no significant induction of apoptosis or senescence of epidermal stem cells during physiological skin ageing.** **a**, Representative immunofluorescence images of CASP3 in the tail scale area from 8-wo and 29-mo wild-type mice. CASP3$^+$ cells were found 1 day after 10 Gy irradiation of dorsal skin (positive control). **b**, Number of CASP3$^+$ cells per basal scale area in positive control, 7–8-wo ($n = 4$) and 25–29-mo ($n = 3$) wild-type mice. The number of CASP3$^+$ cells was not significantly increased in epidermal basal cells from young or aged mice. **c**, Representative immunofluorescence images of p16$^+$ signals in the tail scale area from 7-wo and 29-mo wild-type mice. p16 signals were found in DMBA/TPA-induced mouse papilloma (positive control), but no specific induction of p16 was found in the basal cells of aged mice even at 29 mo. **d**, Number of p16$^+$ cells per 10 μm in skin from positive control, 7-wo ($n = 3$) and 25–29-mo ($n = 3$) wild-type mice. p16$^+$ signals were not significantly increased in epidermal basal cells in aged mice compared to young mice. Mean ± s.e.m.; two-tailed *t*-test (**b**, **d**).

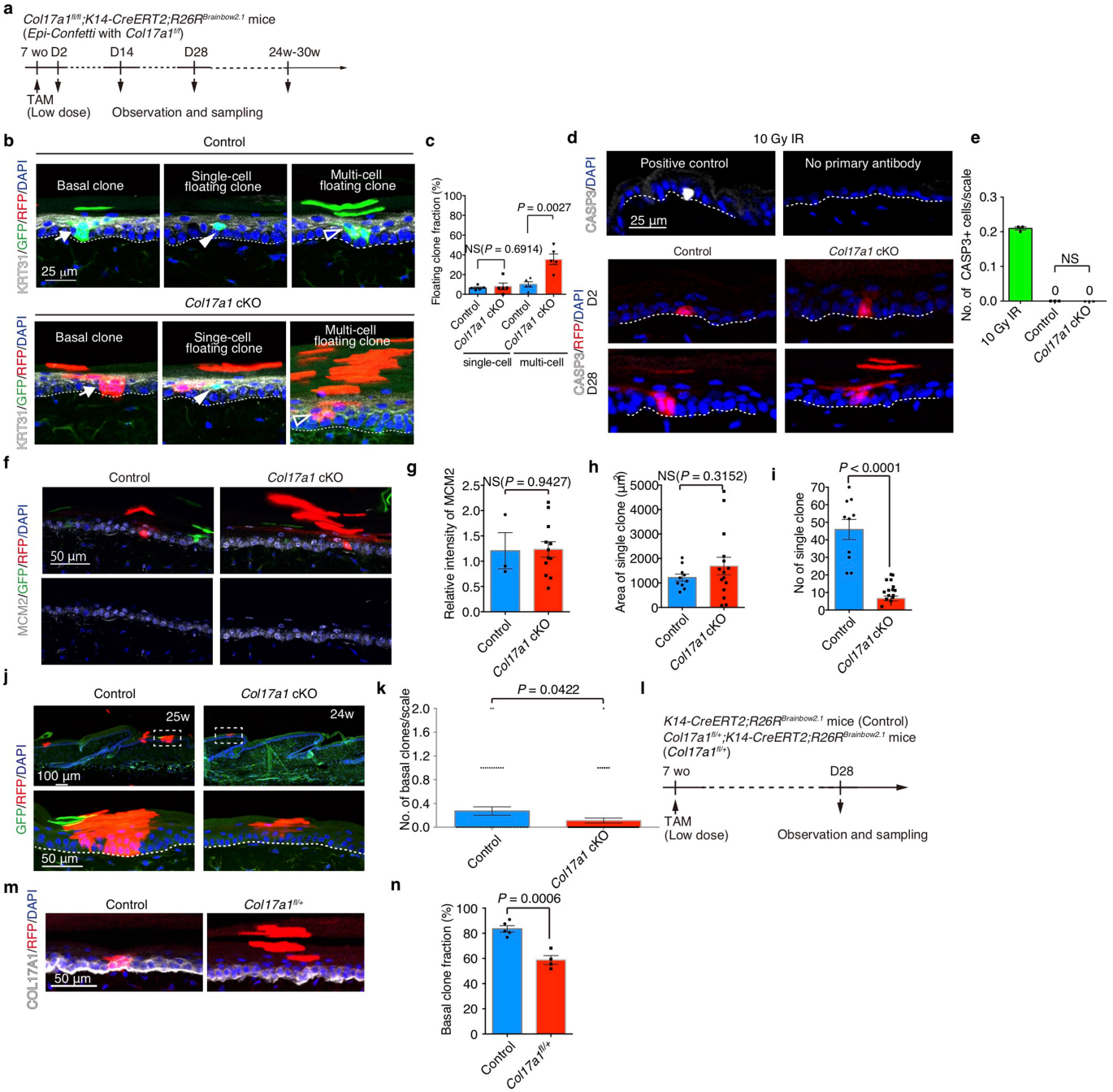


**Extended Data Fig. 5** | See next page for caption.

**Extended Data Fig. 5 | Elimination of *Col17a1*-deficient cells through differentiation-coupled delamination. a**, Experimental design for analysis of stem and progenitor cell fate after deletion of COL17A1. In brief, 7-wo *Col17a1* cKO and control (*Epi-Confetti*) mice were treated with TAM for 1 day (low dose) to label basal keratinocytes at clonal density. Skin samples were collected at D2, D14, D28 and 24–30 weeks (24–30 w). **b**, Representative immunofluorescence images of multicolour-labelled scale basal keratinocytes expressing KRT31 at D28 from control and *Col17a1* cKO mice. Single-cell (arrowhead) or multi-cell floating clones (open arrowhead) were observed. **c**, Frequency of floating clones from control ($n = 5$) and *Col17a1* cKO ($n = 5$) mice in **b**. Multi-cell floating clones were significantly increased during delamination of *Col17a1*-deficient cells. **d**, Representative immunofluorescence images of CASP3 in the tail scale area at 2 and 28 days from TAM-treated control and *Col17a1* cKO mice and at 1 day from 10-Gy-irradiated mice (positive control). Dashed lines, basement membrane. **e**, Number of $CASP3^+$ cells per basal scale area from positive control, control ($n = 3$) and *Col17a1* cKO ($n = 3$) mice. $CASP3^+$ cells were found 1 day after 10 Gy irradiation of dorsal skin but were not found in *Col17a1*-deficient cells during differentiation and delamination. **f**, Representative immunofluorescence images of MCM2 in the tail scale area at 28 days from TAM-treated control and *Col17a1* cKO mice. **g**, Intensity of $MCM2^+$ cells in single-colour clone area from control ($n = 3$ scales) and *Col17a1* cKO ($n = 12$) mice. $MCM2^+$ cells at the non-$G_0$ state did not show any significant difference in *Col17a1*-deficient cells in cKO mice during differentiation or delamination. **h**, **i**, Areas (**h**) and numbers (**i**) of single-colour (red) clones in whole-mount images of tail epidermis at 24–25 w from TAM-treated control ($n = 10$ images) and *Col17a1* cKO ($n = 15$) mice. **j**, Representative immunofluorescence images of multicolour-labelled scale basal keratinocytes at 24–25 w from TAM-treated control and *Col17a1* cKO mice. Bottom, enlarged views of dashed boxed areas shown in top panels. **k**, Number of basal clones per scale in control ($n = 55$ scales) and *Col17a1* cKO ($n = 72$) mice at 24–25 w after TAM administration showing progressive and selective elimination of $Col17a1^-$ cells from the skin. **l**, Experimental design for clonal fate analysis of $Col17a1^{fl/+}$ basal keratinocyte stem and progenitor cells. In brief, 7-wo *Epi-Confetti* $Col17a1^{fl/+}$ and control $Col17a1^{+/+}$ mice were treated with TAM (low dose) to trace the individual stem and progenitor cell-derived clones. Skin samples were collected at D28. **m**, Representative immunofluorescence images of COL17A1 in RFP-expressing basal cells from control and $Col17a1^{fl/+}$ mice. At D28, the $Col17a1^{+/+}$ $RFP^-$ clones replaced the $Col17a1^{fl/+}$ $RFP^+$ basal clones and occupied the basal layer. **n**, Quantification of basal clones in control ($n = 5$) and $Col17a1^{fl/+}$ ($n = 4$) mice at D28 following TAM administration. At D28, basal clones were significantly decreased in number by *Col17a1* heterozygous deficiency. Means ± s.e.m.; two-tailed Mann–Whitney *U*-test (**k**) and two-tailed *t*-test (**c**, **e**, **g**, **h**, **i**, **n**).

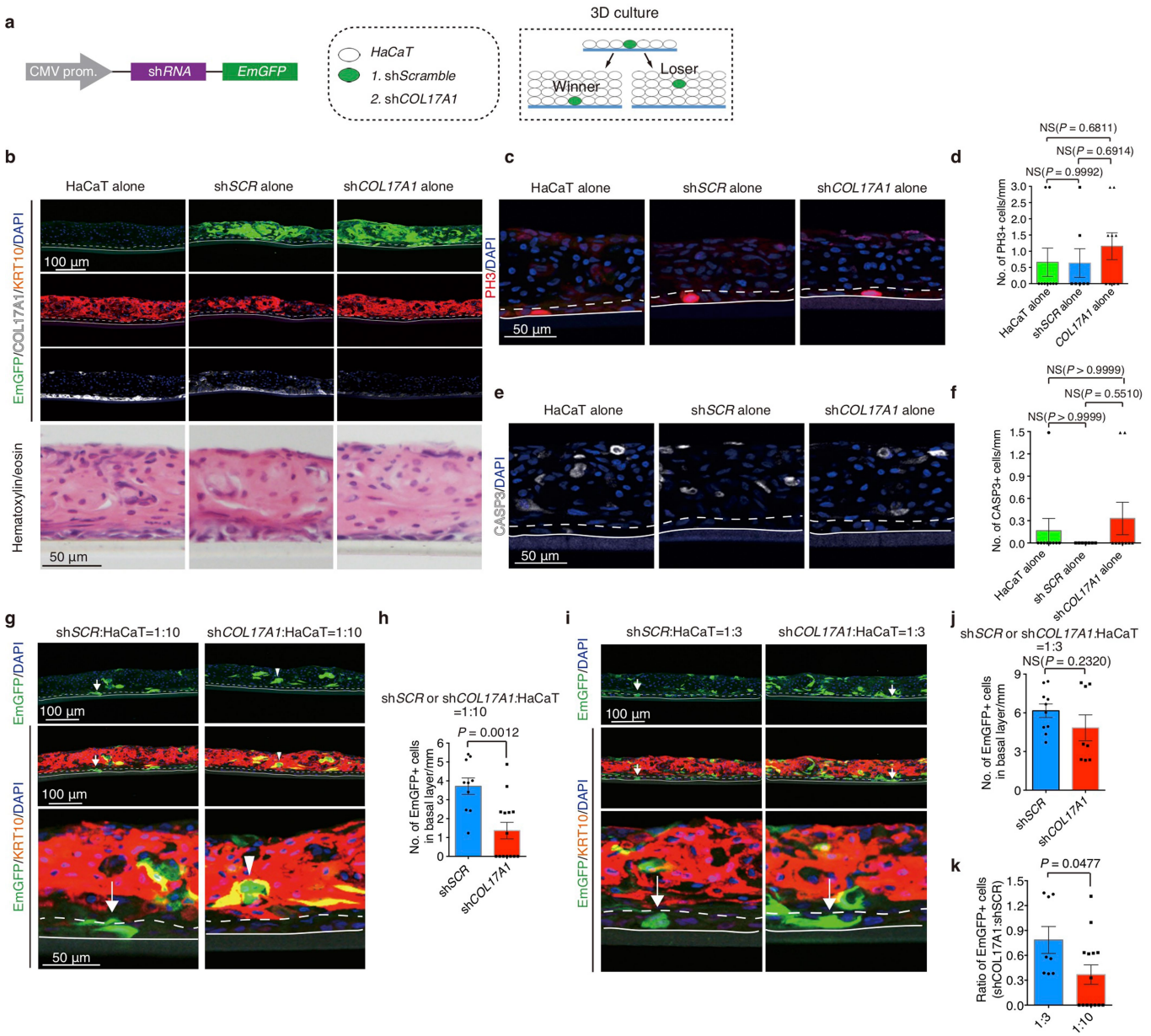


**Extended Data Fig. 6 | COL17A1$^{+}$ basal cells outcompete COL17A1$^{low}$ basal cells in the 3D self-organizing epidermis model. a**, Experimental design for in vitro cell competition assay. Immortalized human HaCaT keratinocytes with inhibitory shRNA (scrambled (sh*SCR*) or sh*COL17A1*) and EmGFP were mixed with EmGFP$^{-}$ parental HaCaT keratinocytes at 1:10, 1:3, 1:0 and 0:1 ratios and were then applied to the 3D culture system for 14 days, after which the competitive contribution of EmGFP$^{+}$ cells in the basal cell layer was analysed. **b**, **g**, **i**, Representative immunofluorescence images of COL17A1, KRT10 and EmGFP and HE images of 3D cultured HaCaT keratinocytes. Three-dimensional cultures with HaCaT or sh*SCR*-expressing cells or sh*COL17A1*-expressing cells alone (**b**) and sh*SCR*- or sh*COL17A1*-expressing EmGFP$^{+}$ cells co-cultured with HaCaT keratinocytes at a 1:10 ratio (**g**) or a 1:3 ratio (**i**) are shown. Dashed lines, boundary of basal layer. In 3D cultures, basal cells express COL17A1 and suprabasal cells express KRT10. Knockdown of *COL17A1* efficiently inhibited COL17A1 expression, but did not affect epidermal stratification and structure (**b**). Arrow, sh*SCR* EmGFP$^{+}$ cells in the basal layer; arrowhead, delaminated sh*COL17A1* EmGFP$^{+}$ cells from the basal layer. **c**, **e**, Representative immunofluorescence images of phospho-histone H3 (PH3) (**c**) or CASP3 (**e**) after 3D culturing alone with HaCaT cells or with sh*SCR* or sh*COL17A1*. **d**, **f**, Quantification of PH3$^{+}$ cells (HaCaT alone, $n = 9$; sh*SCR*, $n = 7$; sh*COL17A1*, $n = 9$ images) (**d**) or CASP3$^{+}$ cells (HaCaT alone, $n = 9$; sh*SCR*, $n = 7$; sh*COL17A1*, $n = 9$ images) (**f**) at the basal layer; there were no significant differences in their frequency among these groups. **h**, **j**, Number of shRNA-expressing EmGFP$^{+}$ cells in the basal cell layer after 3D co-culture with sh*SCR*- or sh*COL17A1*-expressing cells and wild-type HaCaT cells at 1:10 (**h**, sh*SCR*, $n = 10$ images; sh*COL17A1*, $n = 14$ images) or 1:3 (**j**, sh*SCR*, $n = 10$ images; sh*COL17A1*, $n = 8$ images) ratios. **k**, Ratio of sh*COL17A1* or sh*SCR* EmGFP$^{+}$ cells in the basal layer after 3D co-culture with sh*SCR* or sh*COL17A1* EmGFP$^{+}$ and wild-type HaCaT cells at a 1:3 or a 1:10 ratio (1:3, $n = 8$; 1:10, $n = 14$ images). *COL17A1* KD cells were significantly eliminated from the basal layer, depending on the ratio of surrounding wild-type HaCaT cells. Mean ± s.e.m.; one-way ANOVA with Tukey–Kramer post hoc test (**d**), Kruskal–Wallis test with Dunn's post hoc test (**f**) or two-tailed *t*-test (**h**, **j**, **k**).

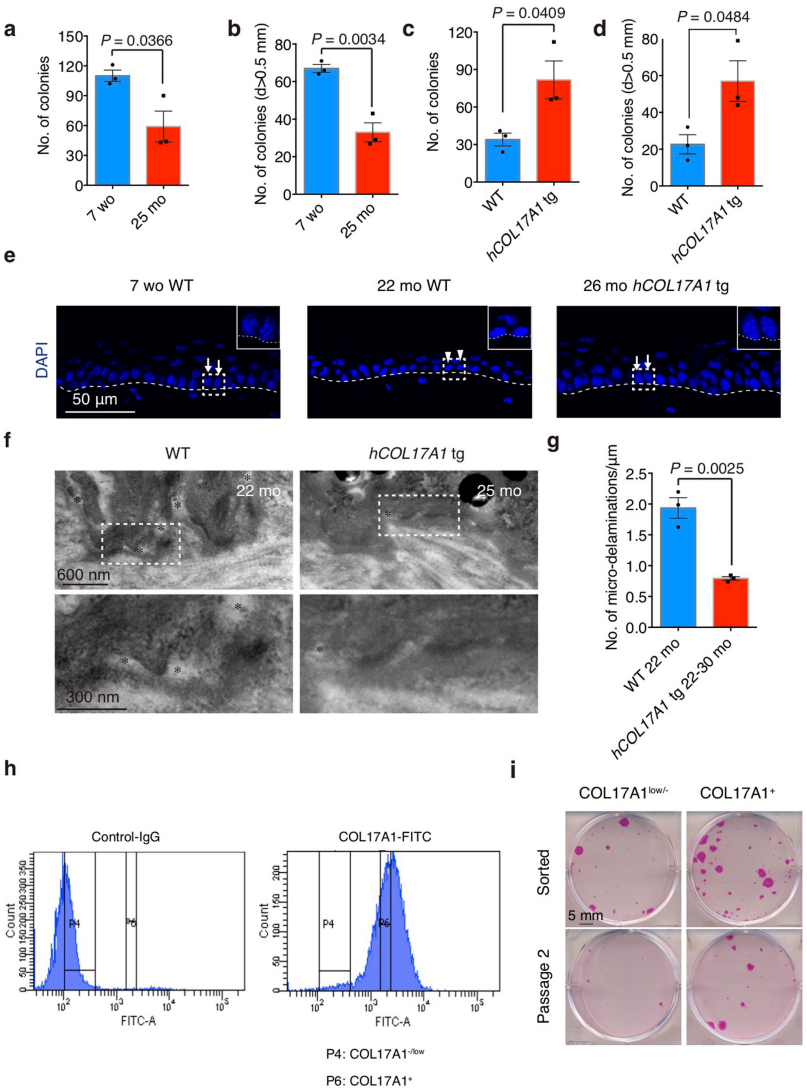


**Extended Data Fig. 7 | Maintenance of COL17A1 enhances epidermal stem cell potential. a–d**, Colony-forming analysis of tail epidermal keratinocytes from young (7 wo, $n = 3$) and aged (25 mo, $n = 3$) mice (**a**, **b**) or from wild-type (8 wo, $n = 3$) and *hCOL17A1* tg (8 wo, $n = 3$) mice (**c**, **d**). Colony number and size were significantly decreased by ageing (**a**, **b**). Expression of the *hCOL17A1* transgene significantly increased the number and size of colonies in primary tail epidermal keratinocytes (**c**, **d**). **e**, Representative immunofluorescence images of DAPI$^+$ nuclei in tail scale IFE from young (7 wo) and aged (22 mo) wild-type mice and from aged (26 mo) *hCOL17A1* tg mice. Young and aged *hCOL17A1* tg tail basal cells show a rectangular and perpendicularly polarized structure against the basement membrane (arrows), whereas many aged tail basal cells show a flattened structure (arrowheads). Insets, magnified views of dashed boxed areas. Similar results were obtained in at least five independent experiments. **f**, Representative ultrastructural images of epidermal basal cells from wild-type (22 mo) and *hCOL17A1* tg (25 mo) mice assessed by TEM. Bottom, enlarged views of dashed boxed areas. Asterisks, micro-delaminations. **g**, Numbers of micro-delaminations at the basement membrane in tail scale basal cells from wild-type (22 mo, $n = 3$) and *hCOL17A1* tg (22–30 mo, $n = 3$) mice. Expression of the *hCOL17A1* transgene significantly decreased age-associated micro-delaminations. **h**, Representative FACS histogram of COL17A1 expression by NHEKs. P4 (COL17A1$^{-/low}$) and P6 (COL17A1$^+$) fractions were collected by a cell sorter. Data are representative of at least two independent experiments. **i**, Colony-forming analysis of COL17A1$^{low/-}$ or COL17A1$^+$ NHEKs with or without serial passage. Data are representative of three independent experiments. Mean ± s.e.m.; two-tailed *t*-test (**a**–**d**, **g**).

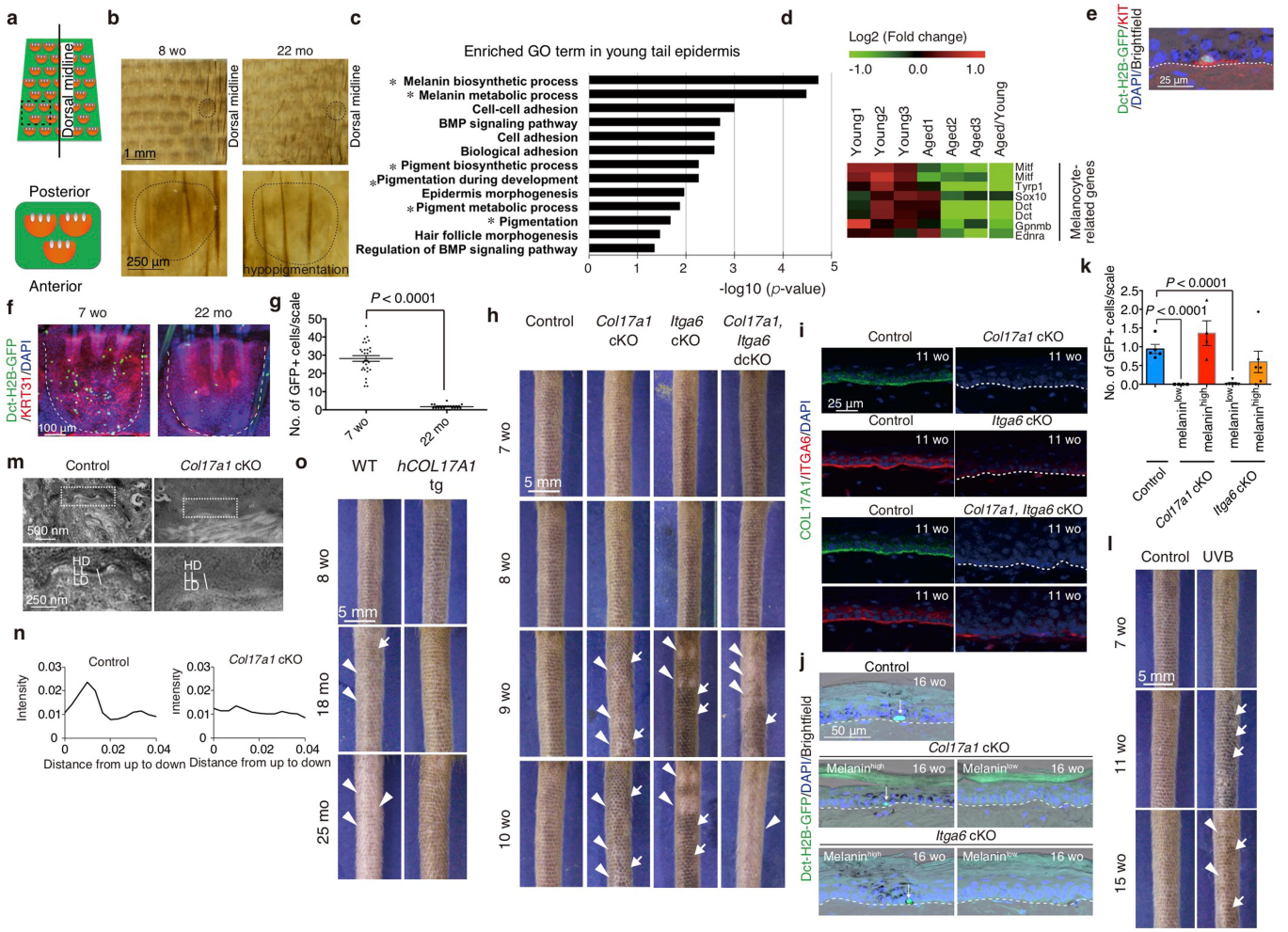


**Extended Data Fig. 8 | Hemidesmosome instability in basal keratinocytes causes epidermal dyspigmentation.** **a**, Schematic of whole-mount views of scale (orange) and interscale (green) areas in mouse tail epidermis. **b**, Representative whole-mount images of pigment distribution in the tail epidermis from young (8 wo) and aged (22 mo) mice; bottom, enlarged views of dashed outlines. Similar results were obtained in at least three independent experiments. **c**, GO analysis between total epidermal cells from young (7–8 wo, $n = 3$) and aged (22–25 mo, $n = 3$) mice for ≥twofold-downregulated genes in aged total epidermal cells. The GO terms for melanocyte-related genes (asterisks) were significantly enriched in young epidermal cells. **d**, Heat map showing the fold change (expressed as a log) between total epidermis from young (7–8 wo, $n = 3$) and aged (22–25 mo, $n = 3$) mice for melanocyte-related genes such as *Mitf*, *Tyrp1*, *Sox10* and *Dct*. **e**, Representative immunofluorescence image of KIT$^+$ melanocytes in Dct–H2B–GFP$^+$ tg mice. Dct–H2B–GFP$^+$ was merged with KIT$^+$ in epidermal melanocytes and melanoblasts. Data are representative of at least ten independent experiments. **f**, Representative tail whole-mount immunofluorescence images of melanocyte distribution and KRT31 expression in skin from 7-wo and 22-mo *Dct-H2B-GFP* tg mice. Dashed line, margin of scale area. **g**, Numbers of GFP-marked melanocytes per scale area from young (7 wo, $n = 29$ scales) and aged (22 mo, $n = 24$) *Dct-H2B-GFP* tg mice. Dct–H2B–GFP$^+$ melanocytes were significantly decreased during ageing. **h**, Representative images of tail skin after deletion of *Col17a1* and/or *Itga6*. We treated 7-wo wild-type (control), *Col17a1* cKO, *Itga6*$^{fl/fl}$;*K14-creERT2* (*Itga6* cKO) or *Col17a1*$^{fl/fl}$;*Itga6*$^{fl/fl}$;*K14-creERT2* (*Col17a1*, *Itga6* dcKO) mice with TAM to delete each gene in epidermal basal keratinocytes. Arrows, hyperpigmentation; arrowheads, hypopigmentation. **i**, Representative immunofluorescence images of COL17A1 and ITGA6 in the tail scale area from cont, *Col17a1* cKO, *Itga6* cKO and *Col17a1*, *Itga6* dcKO (11 wo) mice. Data are representative of at least three independent experiments. **j**, Representative combined immunofluorescence and bright field (melanin$^{high/low}$) images of GFP at 16 wo from control and *Col17a1* or *Itga6* cKO mice. Arrows indicate epidermal melanocytes among tail scale basal keratinocytes. **k**, Numbers of GFP-marked melanocytes per tail scale area (melanin$^{high/low}$) from control ($n = 5$), *Col17a1* cKO ($n = 4$) and *Itga6* cKO ($n = 6$) combined with *Dct-H2B-GFP* tg mice. Melanin$^{high}$ scale areas from *Col17a1* or *Itga6* cKO mice showed no significant difference in the number of GFP-marked melanocytes, whereas melanin$^{low}$ scale areas from *Col17a1* or *Itga6* cKO mice showed a significant decrease in the number of GFP-marked melanocytes. **l**, **o**, Representative images of tail skin from control and UVB-exposed mice at 7 wo, 11 wo and 15 wo (**l**) or wild-type mice and *hCOL17A1* tg mice at 8 wo, 18 mo and 25 mo (**o**). Repetitive UVB exposure induced hyper-pigmentation (arrows) in a month at 11 wo followed by appearance of depigmented spots upon the cessation of UVB irradiation (arrowheads) at 15 wo. Expression of the *hCOL17A1* transgene rescued the age-associated epidermal dyspigmentation. **m**, Representative ultrastructural images of scale basal cells from control (11 wo) and *Col17a1* cKO (11 wo) mice assessed by TEM. Bottom, enlarged views of dashed boxed areas. White lines, show regions across the hemidesmosome, lamina lucida and lamina densa. **n**, Intensity histograms (above lines) for hemidesmosomes in **m**. Similar results were obtained in at least three independent experiments. Images are representative of at least five independent experiments (**h**, **l**, **o**). Mean ± s.e.m.; modified Fisher's exact test (**c**), two-tailed Mann–Whitney *U*-test (**g**) or one-way ANOVA with Dunnett's post hoc test (**k**).

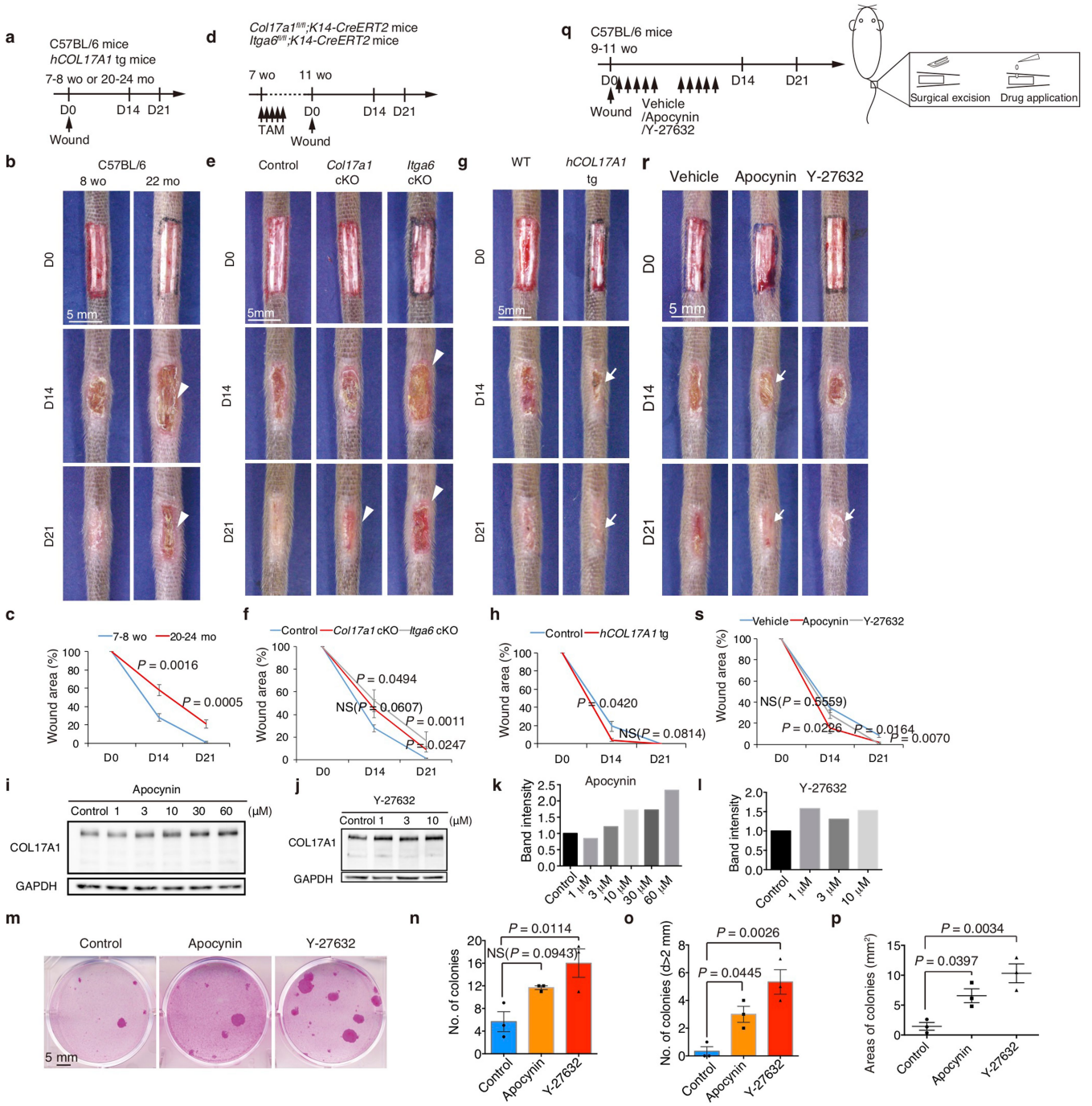


**Extended Data Fig. 9 | Hemidesmosome-mediated lateral stem cell expansion facilitates skin wound healing. a**, **d**, **q**, Experimental designs. Full-thickness wounds were created by skin excision on the tails of young (7–8 wo) and aged (20–24 mo) wild-type mice or of 8-wo wild-type and *hCOL17A1* tg mice (**a**); and of 11-wo wild-type (control), TAM-treated *Col17a1* cKO and *Itga6* cKO mice (**d**). Wound repair processes were observed over time. **q**, Vehicle, apocynin or Y-27632 were repeatedly administered during full-thickness wound healing in wild-type mice (9–11 wo). **b**, **e**, **g**, **r**, Representative images of tail skin wounds from young ($n = 7$) and aged wild-type ($n = 5$) mice (**b**) or from control ($n = 13$), *Col17a1* cKO ($n = 10$) and *Itga6* cKO ($n = 4$) mice (**e**) or from wild-type ($n = 8$) and *hCOL17A1* tg ($n = 6$) mice (**g**) or from mice treated with vehicle ($n = 9$), apocynin ($n = 4$) or Y-27632 ($n = 4$) (**r**) at D0, D14 and D21. Arrowheads, delayed wound repair areas in aged, *Col17a1* cKO or *Itga6* cKO mice. Arrows, facilitated wound healing areas in *hCOL17A1* tg mice or apocynin- or Y-27632-treated mice. **c**, **f**, **h**, **s**, Unrepaired wound area at D0, D14 and D21. Physiological ageing (**c**) or *Col17a1* or *Itga6* deficiency (**f**) significantly delayed wound repair. Expression of the *hCOL17A1* transgene (**h**), or treatment with apocynin or Y-27632 (**s**) significantly facilitated wound repair. **i**, **j**, Western blot analysis of COL17A1 in HaCaT keratinocytes after treatment with vehicle (control), apocynin (**i**) or Y-27632 (**j**). **k**, **l**, Band intensity of COL17A1 relative to GADPH after treatment with apocynin (**k**) or Y-27632 (**l**). Both chemicals significantly induced COL17A1 expression. Similar results were obtained in at least two independent experiments. **m**, Colony-forming analysis of NHEKs after treatment with vehicle (control), apocynin or Y-27632. Data are representative of at least two independent experiments. **n**–**p**, Colony number ($n = 3$ wells) was significantly increased by Y-27632 treatment (**n**), and colony size ($n = 3$ wells) (diameter >2 mm) (**o**) or average size ($n = 3$ wells) of the top five colonies (**p**) was significantly increased by treatment with Y-27632 or apocynin. Means ± s.e.m.; two-tailed *t*-test (**c**, **h**) or one-way ANOVA with Dunnett's post hoc test (**f**, **n**–**p**, **s**).

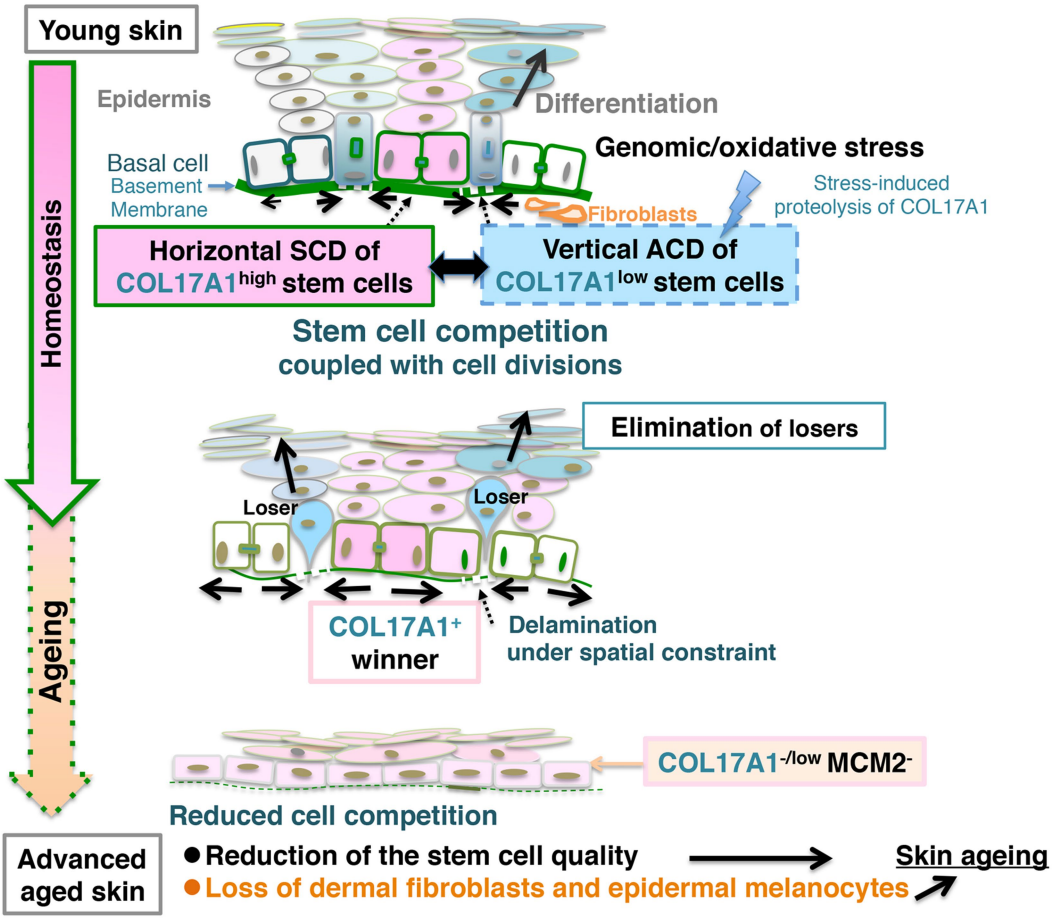


**Extended Data Fig. 10 | A schematic model of epidermal stem cell competition for skin homeostasis and ageing.** Top, homeostatic epidermis. COL17A1$^{+}$ stem cells undergo parallel cell divisions that spread horizontally on the basement membrane and naturally generate the mechanical driving force for cell competition to eliminate COL17A1$^{low/-}$ stressed stem cells in the basal layer because of spatial constraints. Bottom, aged epidermis. Thin, atrophic and fragile skin with basal cells of COL17A1$^{-}$MCM2$^{-}$ exhausted/quiescent state resulting from repetitive stem cell competition and clonal expansion processes in homeostatic epidermis.

nature research

Corresponding author(s): Emi K NIshimura, Hiroyuki Matsumura

# Reporting Summary

Nature Research wishes to improve the reproducibility of the work that we publish. This form provides structure for consistency and transparency in reporting. For further information on Nature Research policies, see Authors & Referees and the Editorial Policy Checklist.

## Statistical parameters

When statistical analyses are reported, confirm that the following items are present in the relevant location (e.g. figure legend, table legend, main text, or Methods section).

| n/a | Confirmed |
|---|---|
| ☐ | ☒ The exact sample size (*n*) for each experimental group/condition, given as a discrete number and unit of measurement |
| ☐ | ☒ An indication of whether measurements were taken from distinct samples or whether the same sample was measured repeatedly |
| ☐ | ☒ The statistical test(s) used AND whether they are one- or two-sided<br>*Only common tests should be described solely by name; describe more complex techniques in the Methods section.* |
| ☒ | ☐ A description of all covariates tested |
| ☐ | ☒ A description of any assumptions or corrections, such as tests of normality and adjustment for multiple comparisons |
| ☐ | ☒ A full description of the statistics including central tendency (e.g. means) or other basic estimates (e.g. regression coefficient) AND variation (e.g. standard deviation) or associated estimates of uncertainty (e.g. confidence intervals) |
| ☐ | ☒ For null hypothesis testing, the test statistic (e.g. *F*, *t*, *r*) with confidence intervals, effect sizes, degrees of freedom and *P* value noted<br>*Give P values as exact values whenever suitable.* |
| ☒ | ☐ For Bayesian analysis, information on the choice of priors and Markov chain Monte Carlo settings |
| ☒ | ☐ For hierarchical and complex designs, identification of the appropriate level for tests and full reporting of outcomes |
| ☐ | ☒ Estimates of effect sizes (e.g. Cohen's *d*, Pearson's *r*), indicating how they were calculated |
| ☐ | ☒ Clearly defined error bars<br>*State explicitly what error bars represent (e.g. SD, SE, CI)* |

*Our web collection on statistics for biologists may be useful.*

## Software and code

Policy information about availability of computer code

| | |
|---|---|
| Data collection | FV10-ASW4.2 Software version 4.02 (Olympus) was used for capturing confocal images. BD FACS Diva Software version 6.1.3 (BD Bioscience) were used for collecting FACS data. Fusion Software (Vilber lourmat) were used for collecting western-blot data. |
| Data analysis | For statistical analysis, Excel 2015 (Microsoft Corp.) and GraphPad PRISM 6 (GraphPad Software, Inc.) were used. For image analysis, Image J Fiji was used. For microarray data analysis, TIGRMeV software (version 4.8.1, http://mev.tm4.org/#/welcome), the web-based Database for Annotation, Visualization and Integrated Discovery (DAVID) 6.7 were used. |

For manuscripts utilizing custom algorithms or software that are central to the research but not yet described in published literature, software must be made available to editors/reviewers upon request. We strongly encourage code deposition in a community repository (e.g. GitHub). See the Nature Research guidelines for submitting code & software for further information.

## Data

Policy information about availability of data

All manuscripts must include a data availability statement. This statement should provide the following information, where applicable:

- Accession codes, unique identifiers, or web links for publicly available datasets
- A list of figures that have associated raw data
- A description of any restrictions on data availability

Microarray data were deposited in Gene Expression Omnibus (www.ncbi.nlm.gov/geo/) under series identifier GSE111825.
All other data that support the conclusions are available from the authors on request.

# Field-specific reporting

Please select the best fit for your research. If you are not sure, read the appropriate sections before making your selection.

☒ Life sciences ☐ Behavioural & social sciences ☐ Ecological, evolutionary & environmental sciences

For a reference copy of the document with all sections, see nature.com/authors/policies/ReportingSummary-flat.pdf

# Life sciences study design

All studies must disclose on these points even when the disclosure is negative.

| | |
|---|---|
| Sample size | Preliminary experiments were performed to determine the sample size. Sample size sufficiency were determined by previous experiments from our laboratory. No statistical methods were used to predetermine the sample size. |
| Data exclusions | For wound healing experiments, the mice with abnormal wounds (by fighting or physical interaction) were excluded. The mice, which have atypical wound with physical interaction were excluded through the careful daily observation. |
| Replication | All attempts at replication were successful. |
| Randomization | The experiments were not randomized |
| Blinding | We were not blinded to allocation during experiments and outcome assessment. But, another lab investigators repeatedly performed similar experiments to confirm the reproducibility especially in Extened Data Fig. 9. |

# Reporting for specific materials, systems and methods

### Materials & experimental systems

| n/a | Involved in the study |
|---|---|
| ☒ | ☐ Unique biological materials |
| ☐ | ☒ Antibodies |
| ☐ | ☒ Eukaryotic cell lines |
| ☒ | ☐ Palaeontology |
| ☐ | ☒ Animals and other organisms |
| ☐ | ☒ Human research participants |

### Methods

| n/a | Involved in the study |
|---|---|
| ☒ | ☐ ChIP-seq |
| ☐ | ☒ Flow cytometry |
| ☒ | ☐ MRI-based neuroimaging |

## Antibodies

Antibodies used

For IHC, Guinea pig antibody to KRT31 (Progen, GP-hH1, 1:50 for whole-mount immunostaining, 1:100 for frozen-section immunostaining); rabbit antibody to MCM2 (Abcam, ab31159, 1:300); rabbit antibody to COL17A1 (Abcam, ab186415, 1:50 for whole-mount immunostaining, 1:200 for frozen-section immunostaining); rat antibody to ITGA6 (BD Pharmingen, 555734,1:50 for whole-mount immunostaining, 1:150 for frozen-section immunostaining); guinea pig antibody to PLECTIN (Progen, gp21, 1:100); rabbit antibody to COL7A1 (Millipore, 234192, 1:100); mouse antibody to ITGB1 (Miltenyi Biotech, 130-096-309,1:100); rat antibody to ITGB4 (BD Pharmingen, 553745); rat antibody to KIT (BD Pharmingen, 553868); rat antibody to COL17A1 (Clone 8B6E9, Nishimura laboratory, 1:50); rat antibody to PH3 (Sigma-Aldrich, H9908, 1:150); rabbit antibody to Caspase 3 (Cell Signaling, 9661, 1:200); chicken antibody to GFP (Abcam, ab13970, 1:300); mouse antibody to KRT10 (Santa Cruz Biotechnology, SC-52318, 1:200); rabbit antibody to Survivin (Cell Signaling, 2808, 1:150); rat antibody to PDGFRa (eBioscience, 14-1401, 1:150); rabbit antibody to phospho histone H2AX (Cell Signaling, 1:150); rabbit antibody to DCT (a kind gift from Dr. Vincent Hearing,

National Cancer Institute, 1:150); mouse antibody to 8-OHdG (Abcam, 1:2000); rabbit antibody to p-RPA2/32 (Abcam, 1:150);
For WB, Mouse monoclonal antibody to human COL17A1 (COVANCE, SIG-3780, 1:100); mouse monoclonal antibody against PLECTIN (Cosmo Bio, NU-01-PLC, 1:200); rabbit polyclonal antibody against ITGA6 (Abcam, ab97760, 1:1000); rabbit polyclonal antibody against ITGB4 (Santa Cruz Biotechnology, sc-9090, 1:1000); rabbit monoclonal antibody against ITGB1 (Abcam, ab179471, 1:2000),rabbit monoclonal antibody to phospho histone H2AX (Cell Signaling, 1:1000), rabbit polyclonal antibody to αβ-tubulin (Cell Signaling, 2148, 1:1000); rabbit monoclonal antibody to GAPDH (Cell Signaling, 2118, 1:5000); mouse monoclonal antibody against β-actin (Sigma, A5441, 1:15000).
For FACS, rabbit monoclonal antibody against COL17A1 (Abcam, ab184996,1:50)

Secondary antibodies used included:
For IHC, Alexa Fluor 488 donkey antibody to rat immunoglobulin (IgG) (Invitrogen-Molecular Probes, A21208, 1:200); Alexa Fluor 488 donkey antibody to mouse IgG (Molecular Probes, A21202, 1:200); Alexa Fluor 488 donkey antibody to chicken IgY (Jackson Immuno Research Laboratories, Inc., 703-545-155, 1:200); Alexa Fluor 568 goat antibody to guinea pig IgG (Molecular Probes, A11075, 1:200); Alexa Fluor 594 donkey antibody to rat IgG (Jackson, 712-585-153, 1:200); Alexa Fluor 594 donkey antibody to rabbit IgG (Molecular Probes, A21207, 1:200); Dylight 594 donkey antibody to mouse IgG (Jackson, 715-515-150, 1:200); Alexa Fluor 680 donkey antibody to rabbit IgG (Molecular Probes, A10043, 1:200); biotinylated goat anti-rabbit immunoglobulin G antibody (Vector Laboratories, BA-1000, 1:200).
For WB, horseradish peroxidase (HRP) conjugated antibody to mouse IgG (GE healthcare #NA934, 1:5000) ; HRP conjugated antibody to rabbit IgG (GE #NA931, 1:5000).
For FACS, ;Normal rabbit IgG (Santa Cruz Biotechnology, 1:50) and Alexa Fluor 488-conjugated rabbit polyclonal antibody (Molecular Probes, A27034, 1:50).

Validation

Antibodies were validated as noted on manufacturer's website. Additional validation was done by the use of negative control (1st ab exclusion or knockout) and control tissue samples for IHC, by the use of negative control (siRNA mediated Knock-down) and control cell lysates for WB and by the use of negative control (control IgG) and control cells for FACS.

## Eukaryotic cell lines

Policy information about cell lines

Cell line source(s)

HaCaT from ATCC (Manassas, VA, USA),
Normal human epidermal keratinocytes (NHEKs) from Kurabo (Osaka, Japan)

Authentication

All cell lines were authenticated by the vendor by morphology check and growth curve analysis. The cell lines were purchased from commercial vendors listed above.

Mycoplasma contamination

Cell lines were routinely tested and found negative for mycoplasma infection by the venders.

Commonly misidentified lines
(See ICLAC register)

No commonly misidentified cell lines were used.

## Animals and other organisms

Policy information about studies involving animals; ARRIVE guidelines recommended for reporting animal research

Laboratory animals

For analysis of wild type mice, C57BL/6N line was used. All transgenic and mutant mice (K14-CreERT2, Dct-H2B-GFP mice; Col17a1 floxed mice; Itga6 floxed mice;Keratin14-human COL17A1 transgenic mice and R26RBrainbow2.1 mice) were backcrossed to C57BL/6J. Both male and female mice (7 weeks to 30 months old) were used.

Wild animals

This study did not involve wild animals.

Field-collected samples

This study did not involve samples collected from the field.

## Human research participants

Policy information about studies involving human research participants

Population characteristics

Potential research participants who agreed with the use of their skin tissue samples collected for diagnostic or therepiutic purposes of skin diseases for research purposes. Aged group (>70 -year-old) and young group (<35-year-old) were randomly chosen from the potential sample lists.

Recruitment

Research participants were recruited from patients who agreed with the research use of their skin samples collected for diagnosstic or therapeutic purposes in a questionnaire. The methods and procedures for recruitment including the questionnaire for potential participants had been approved by the IRB.

# Flow Cytometry

## Plots

Confirm that:

☒ The axis labels state the marker and fluorochrome used (e.g. CD4-FITC).

☒ The axis scales are clearly visible. Include numbers along axes only for bottom left plot of group (a 'group' is an analysis of identical markers).

☒ All plots are contour plots with outliers or pseudocolor plots.

☒ A numerical value for number of cells or percentage (with statistics) is provided.

## Methodology

| | |
|---|---|
| Sample preparation | To generate stable EmGFP high HaCaT cells, pCMV-EmGFP-miR-SCRAMBLE (pcDNA6.2-GW/EmGFP-miR neg control) and pCMV-EmGFP-miR-COL17A1 were transfected into HaCaT cells with Fugene HD reagent (Promega) according to the manufacturer's instructions. The cells were then selected with 5ug/ml blasticidin S solution (Wako) for 14 days. EmGFP high cells were sorted out using a FACSAria II (BD Bioscience).<br>To perform the colony forming analysis from COL17A1+ or COL17A1 low/- keratinocyte fraction, human normal keratinocytes (NHEKs) were grown for 7 days in culture. The cells were tripsinized and resuspended in 2% fetal bovine serum (FBS) in PBS, and incubated with a rabbit monoclonal antibody against COL17A1 (1:50, Abcam) for 1 h on ice, after which the cells were incubated with an Alexa Fluor 488-conjugated rabbit polyclonal antibody (1:50, Molecular Probes) for 1 hr on ice. After washing with 2% FBS in PBS, cells were resuspended in culture medium. Then, COL17A1+ or COL17a1 low/- keratinocyte were sorted sorted out using a FACSAria IIIu (BD Bioscience). |
| Instrument | BD FACSAria II (BD Biosciences) and BD FACSAria IIIu (BD Biosciences) |
| Software | FACSDiva and FACSAria software (BD Biosciences) |
| Cell population abundance | Fluorescent microscopic detection, over 95%. |
| Gating strategy | In HaCaT, Living cells were selected by forward scatter, side scatter, doublets discrimination and by 7AAD dye exclusion. EmGFP high living cells were sorted.<br>In NHEK, Living cells were selected by forward scatter, side scatter, doublets discrimination and by 7AAD dye exclusion. COL17A1 + or COL17a1 low/- living cells were sorted. |

☒ Tick this box to confirm that a figure exemplifying the gating strategy is provided in the Supplementary Information.